Institut für
Kontinuumsmechanik

Leibniz
Universität
Hannover

Computational methods for fracture and applications to the design of new polymeric matrix composites

Xiaoying Zhuang

GRK1462 Summer School
Weimar
Sep 7 2016

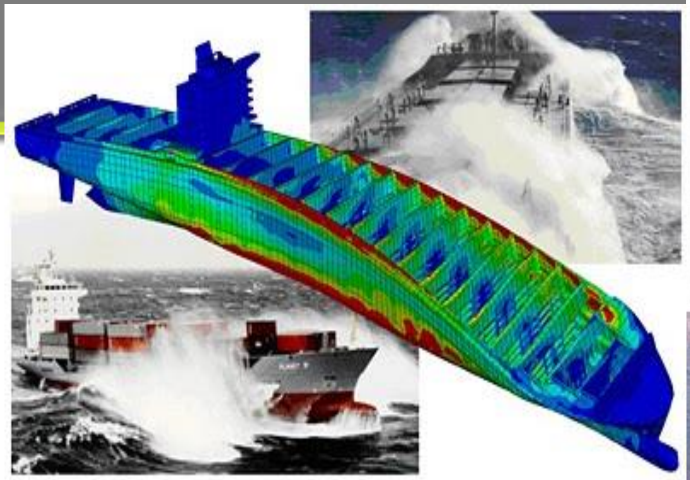

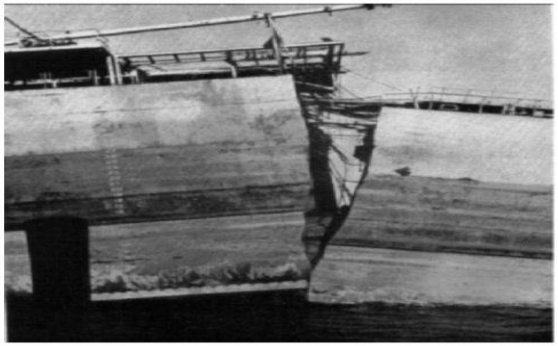

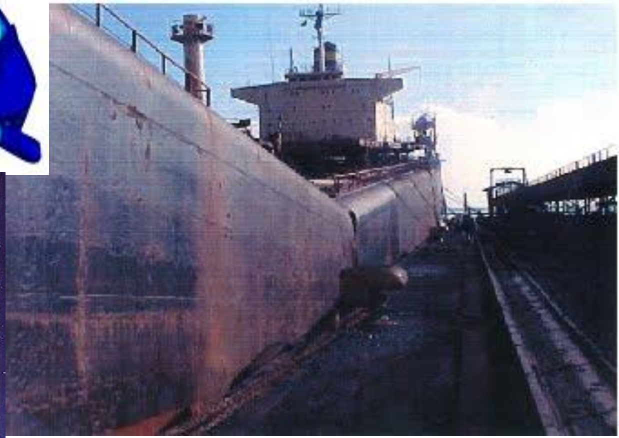


15-A
STB'D

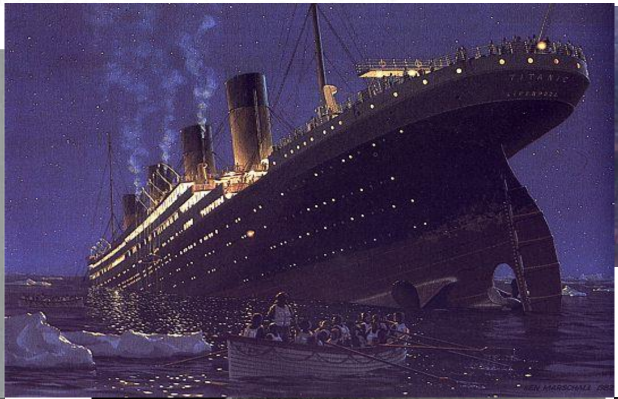

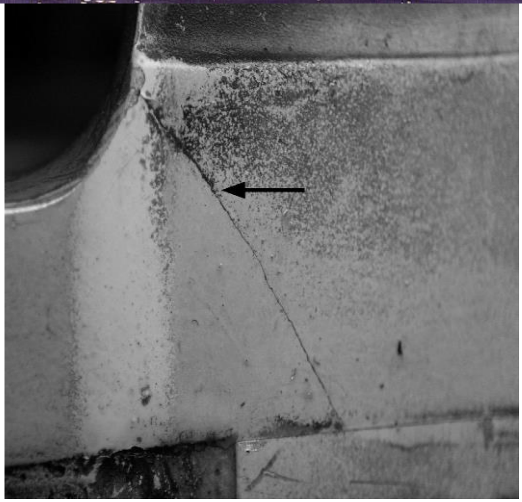

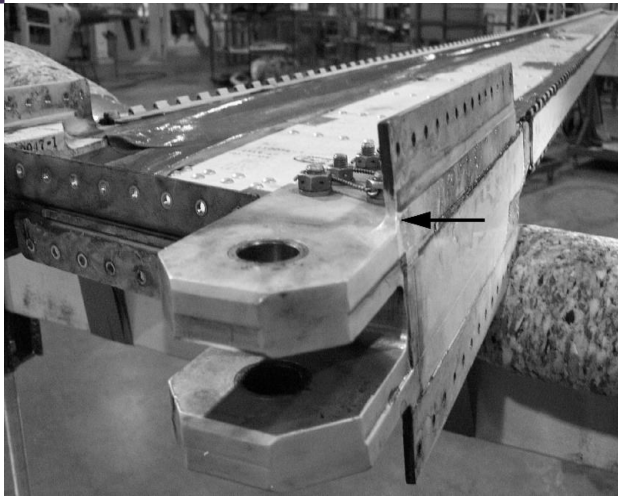

Motivation

- Goal: Prediction of material/structural failure -> cracks (initiation, propagation, branching, junction)

- Is it necessary to model the crack explicitly?

- How can a crack be modeled?
  - Method that describes the crack kinematics
  - Physical condition in order to initiate or propagate a crack

Motivation

Motivation

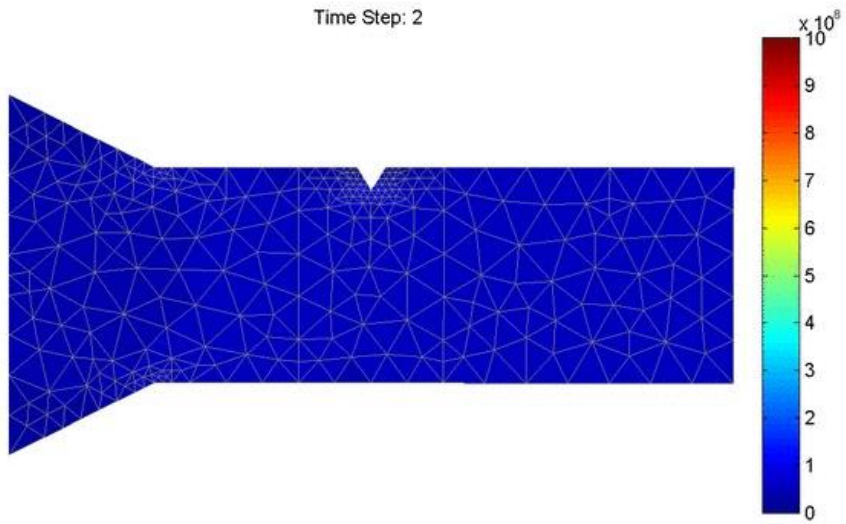

Moes N.,Dolbow J., Belytschko T.: A finite element method for crack growth without remeshing. International Journal for Numerical Methods in Engineering, 1999, 46(1) 133-150

Zhang, Ch., Gao, X.-W., Sladek, J. and Sladek, V.: Fracture Mechanics Analysis of 2-D FGMs by a Meshless BEM. Key Engineering Materials, Vols. 324-325, pp. 1165-1172, 2006.

Areias P., Rabczuk T., Camanho P.P.: Initially rigid cohesive laws and fracture based on edge rotations, Computational Mechanics, 2013, 52(4):931 - 947

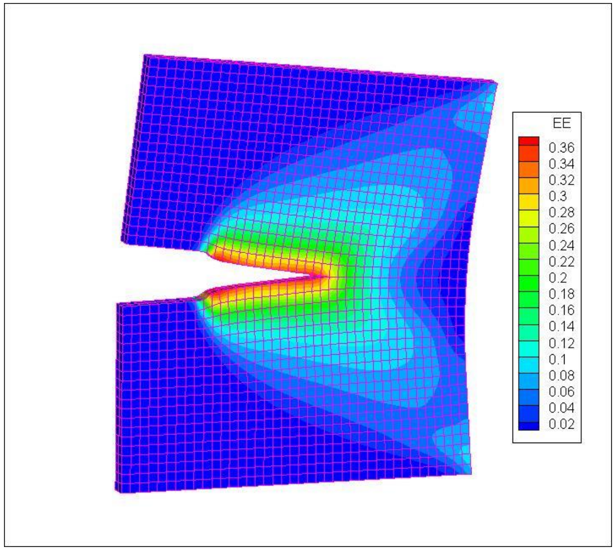

Meshfree methods and particle methods
Meshfree methods for moving boundaries

Xu X.P., Needleman A.: Numerical simulations of fast crack growth in brittle solids. Journal of the Mechanics and Physics of Solids, **1994**, 42:1397-1434
Silling S.A.: Reformulation of elasticity theory for discontinuities and long-range forces, Journal of the Mechanics and Physics of Solids, **2000**, 48(1): 175-209
Sulsky D., Chen Z. Schreyer H.L.: A particle method for history-dependent materials, *Computer Methods in Applied Mechanics and Engineering*, **1994**, 118, 179-196
Rabczuk T., Belytschko T.: Cracking Particles, a simplified meshfree method for arbitrary evolving cracks, 2004,
Pandolfi A., Ortiz M.; An eigenerosion approach to brittle fracture, International Journal for Numerical Methods in Engineering, **2012**, 92, 694-714

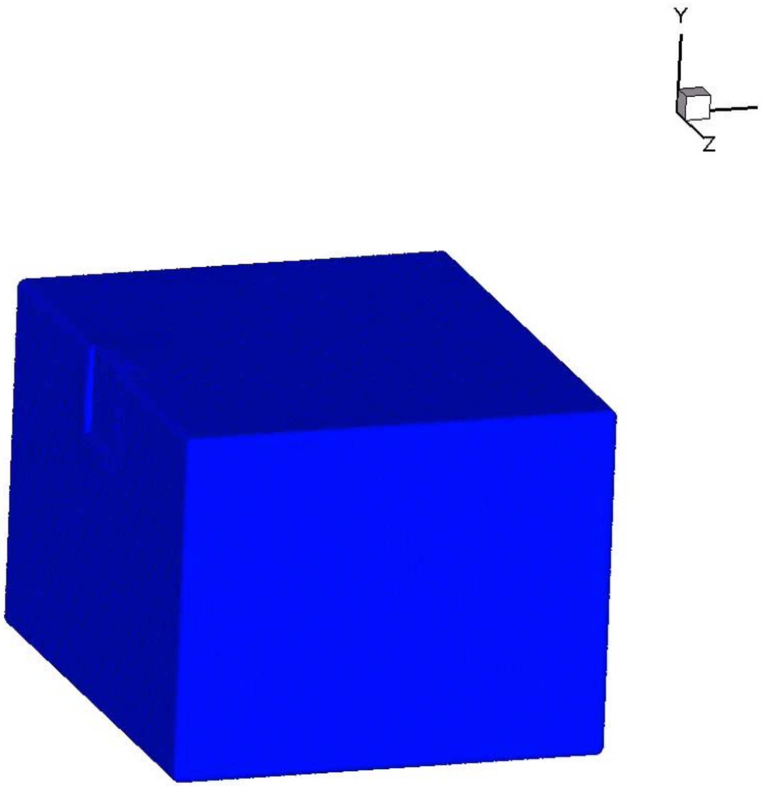

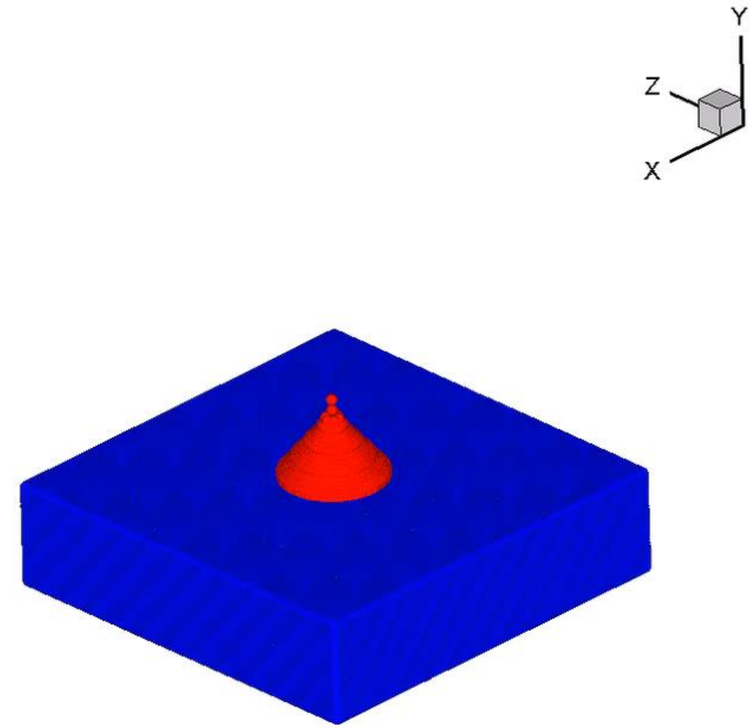

Overview

- Computational Methods for Fracture
    - Meshfree and Particle Methods
    - Peridynamics
- Application to the design of polymer-matrix composites
    - Framework
    - Models at different length scales
    - Multiscale approach

Why meshfree methods?

Advantages:

-Implementation of h-adaptivity is extremely simple
-Can handle large deformations with ease without loss of accuracy
-Higher continuous approximation
-No jumps in the stress/strain field which yields better accuracy compared to FEM
-No need for mesh generation
-No mesh alignment sensitivity due to isotropic character of the meshfree shape functions

Meshfree approximation (NOT interpolation)

FE

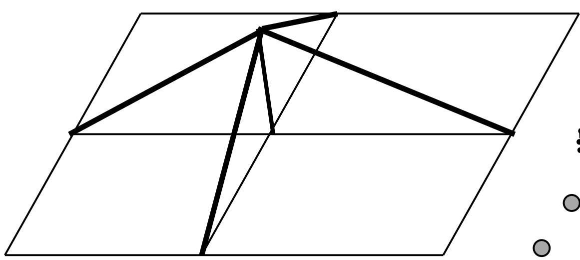

Meshfree

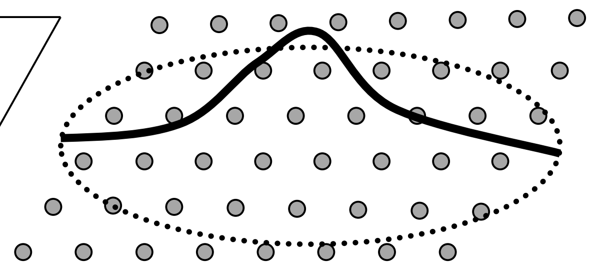

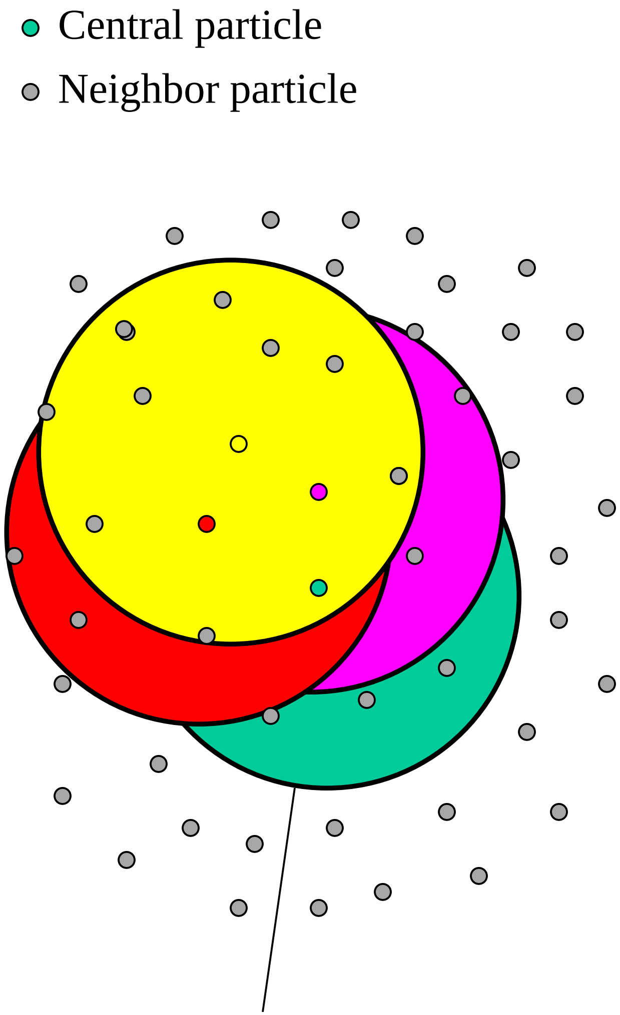

Domain of influence (support)

Meshfree approximation

$$u(\boldsymbol{X}) = \sum_{J \in S} u_J \, \Phi_J(\boldsymbol{X})$$

Meshfree approximation (NOT interpolation)

Basic approximation

$$u(\boldsymbol{X}) = a_i(\boldsymbol{X})\, p_i(\boldsymbol{X}) = \boldsymbol{a}^T \boldsymbol{p}, \quad p = [1\ X\ Y\ Z]$$

Minimize quadratic form

$$S(\boldsymbol{a}(\boldsymbol{X})) = \sum_J w(\boldsymbol{X} - \boldsymbol{X}_J)\left(\boldsymbol{a}^T(\boldsymbol{X})\, \boldsymbol{p}(\boldsymbol{X}_J) - u_J\right)^2$$

leads to linear equations for $\boldsymbol{a}$

can be written in shape function form

$$u(\boldsymbol{X}) = \sum_{J \in S} u_J\, \Phi_J(\boldsymbol{X})$$

Central particle
Neighbor particle

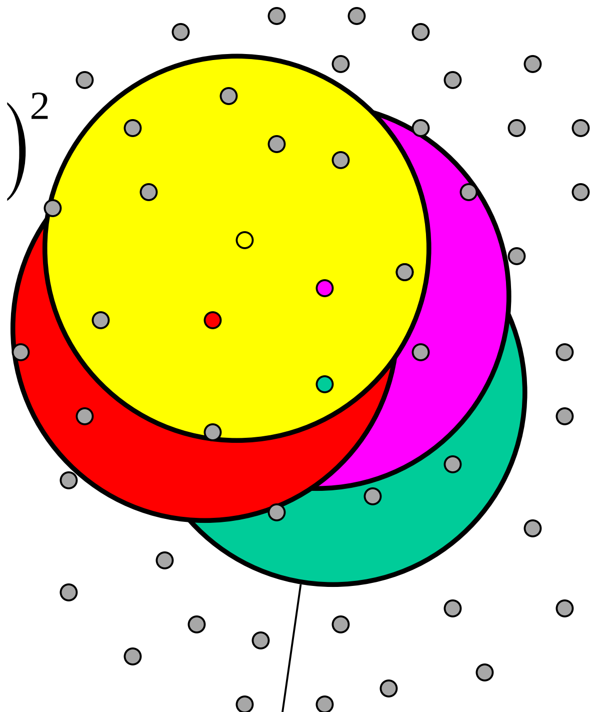

Domain of influence (support)

Meshfree approximation (NOT interpolation)

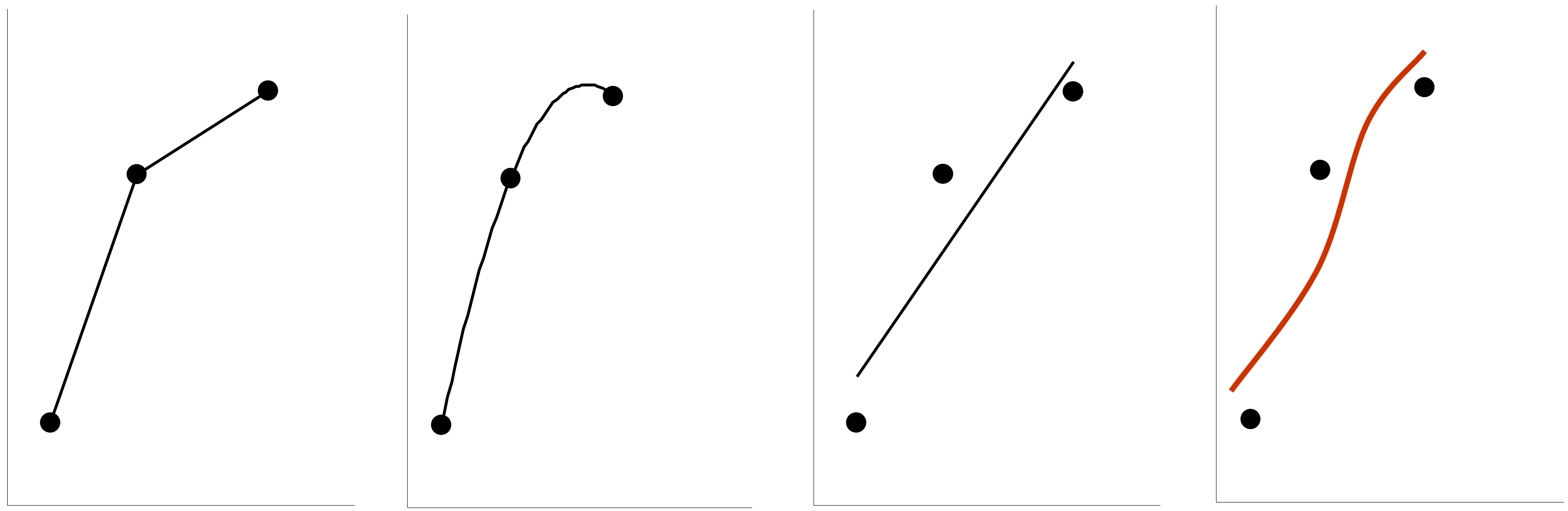

Linear interpolation

Quadratic interpolation

Least squares (linear basis)

Moving least squares (linear basis)

Finite elements

Meshfree methods

$$u^h(\mathbf{x}) = \sum_{I}^{n} \phi_I(\mathbf{x}) u_I$$

Meshfree approximation (NOT interpolation)

-Crack representation in 3D based on level sets

-Efficient integration strategy at the crack front

-Evaluation of the interaction integral in 3D

Representation of crack geometry

Triangular facets have been used to explicitly represent a crack surface (e.g Duflot (2006) & Bordas *et al.* (2008)). However, the accuracy of the modelled crack geometry is reduced. For instance, a penny-shaped crack, which is a smooth curve, must be modelled as straight line segments which are C^0 only.

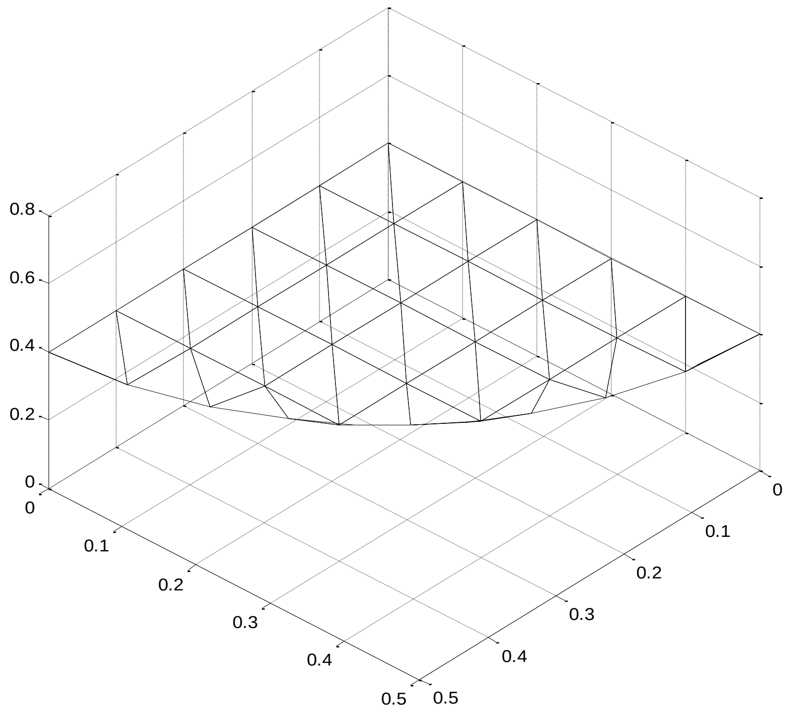

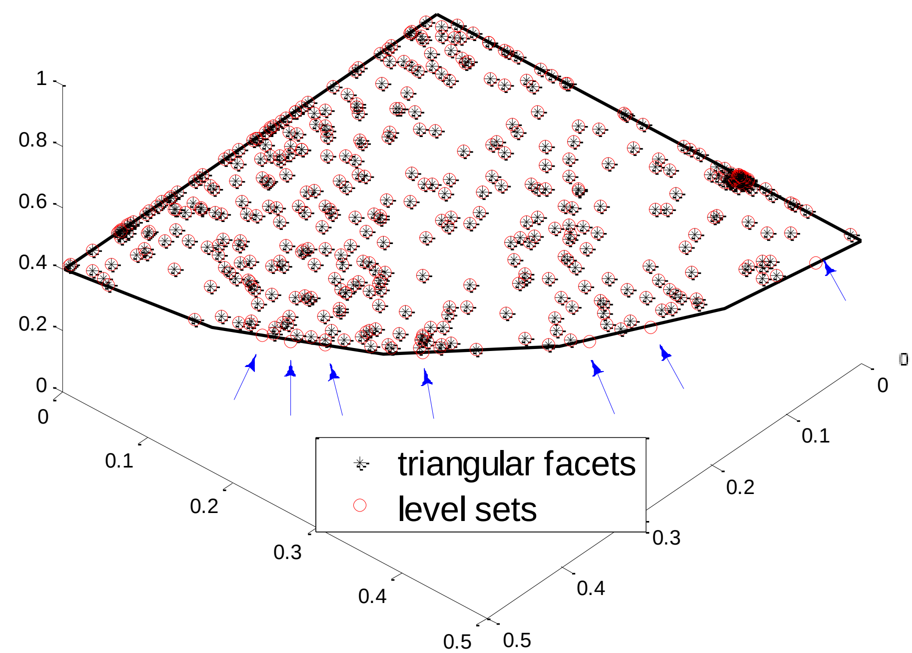

Triangular facets for a penny-shaped crack

Curvature along crack front is omitted

Representation of crack geometry

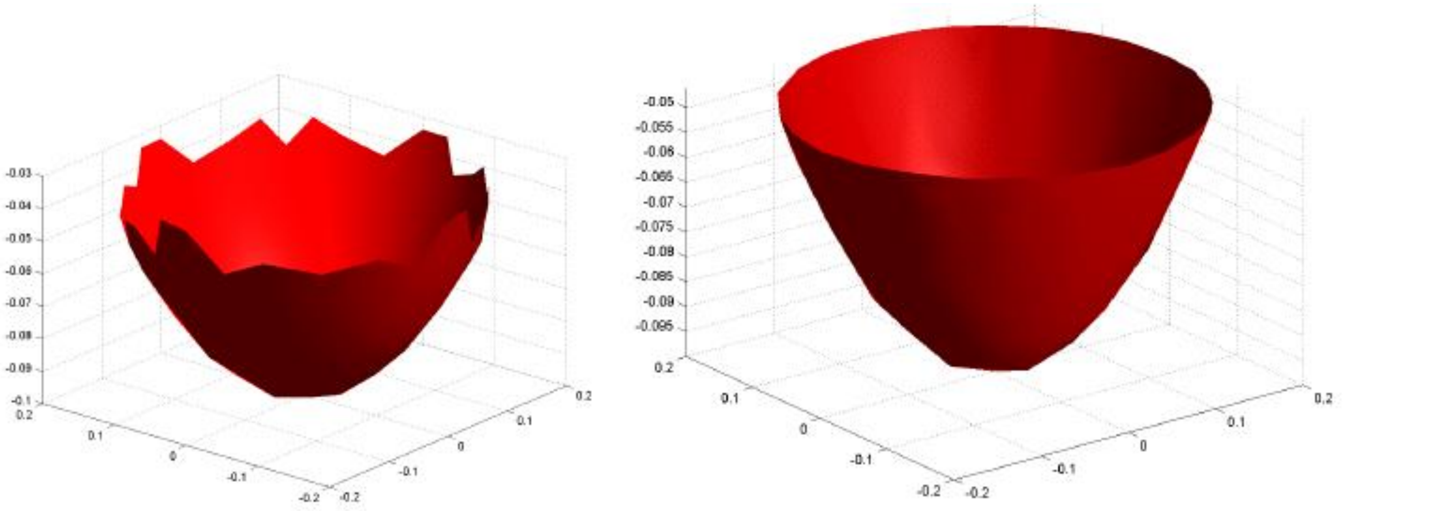

(a) By direction interpolation. (b) By gradient projection method

A comparison of the crack front found by the direction interpolation and gradient projection method for the lens shaped crack.

Zhuang, Augarde, Mathisen. International Journal for Numerical Methods in Engineering, Fracture modelling using meshless methods and level sets in 3D: framework and modelling, 92:969-998, 2012.

Level sets for 3D fracture

The level sets are particularly advantageous for dealing with arbitrary cracks in 3D, which have curvature both in surface and along the crack front.

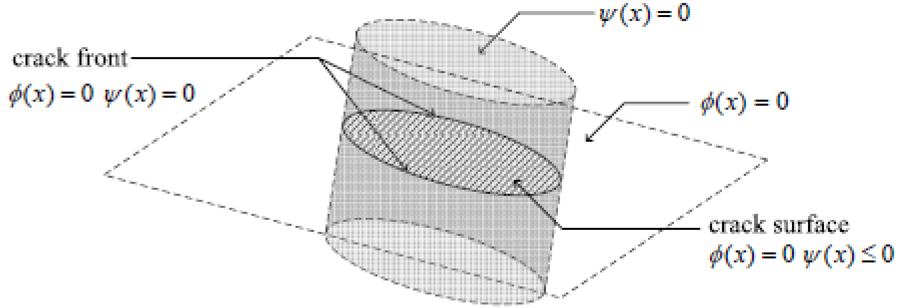

$$\phi(\mathbf{x}) = 0 \quad \psi(\mathbf{x}) \leq 0 \quad \text{crack surface}$$
$$\phi(\mathbf{x}) = 0 \quad \psi(\mathbf{x}) = 0 \quad \text{crack front}$$

Level sets are advanced by solving the H-J equation:

$$\frac{\partial \phi(\mathbf{x})}{\partial t} + v_\phi \nabla\phi(\mathbf{x}) \cdot \nabla\phi_0(\mathbf{x}) = 0$$

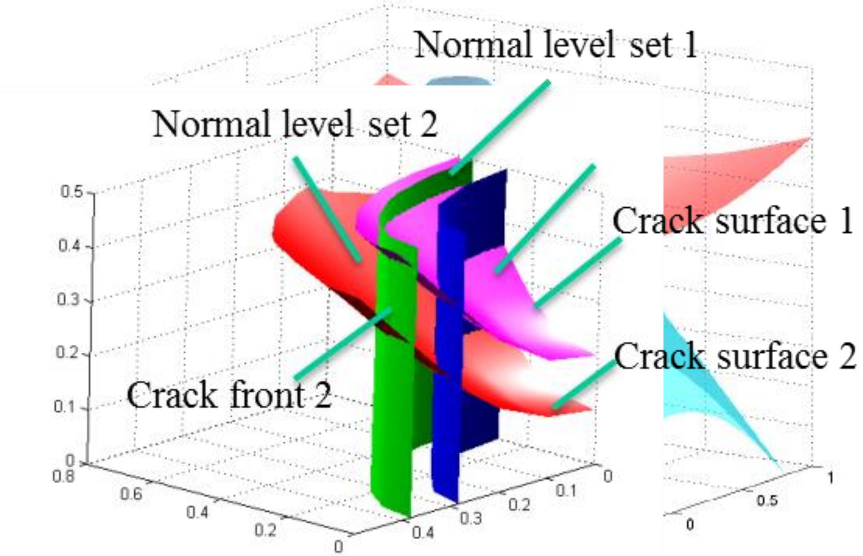

ϕ and ψ of a lens-shaped crack

Shear-compression crack propagation

The crack growth path of offset joints

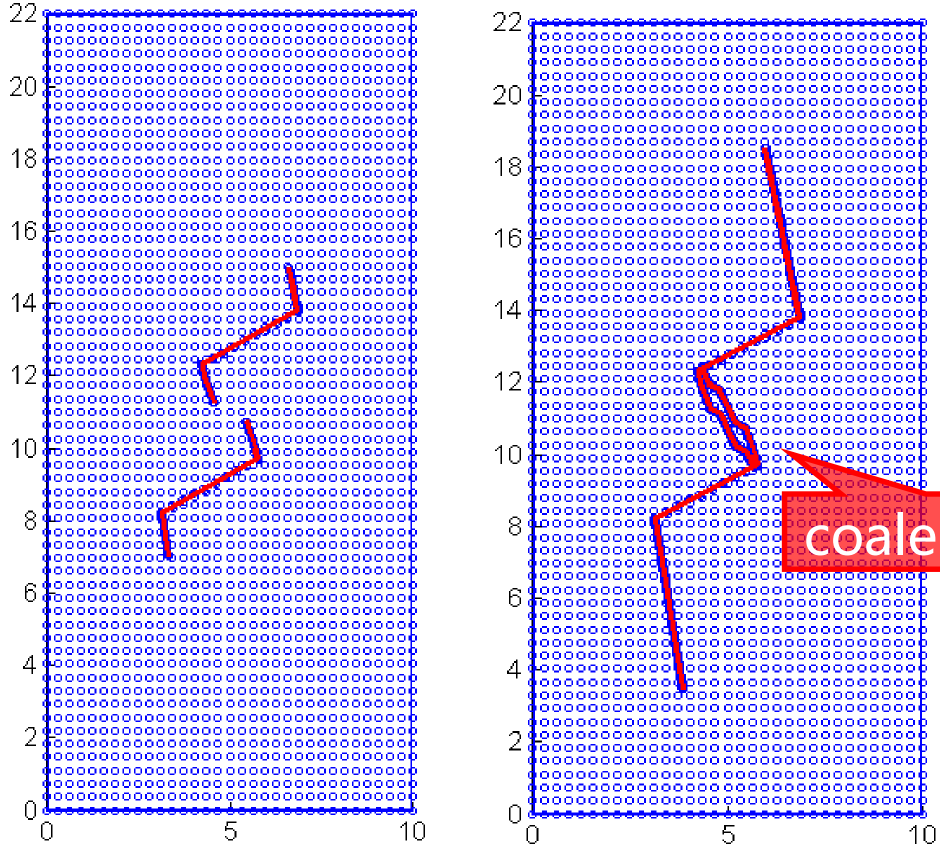

coalescence

Zhuang, Huang, Zhu (2012)

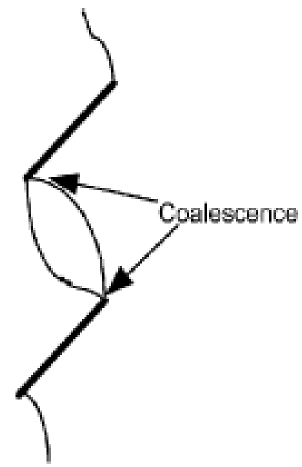

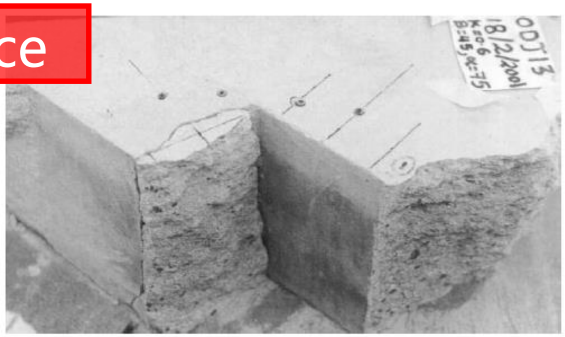

MUGHIEDA et al. (2004) [Geotechnical and Geological Engineering]

Meshfree approximation (NOT interpolation)

My contributions:

-Crack representation in 3D based on level sets

-Efficient integration strategy at the crack front

-Evaluation of the interaction integral in 3D

Singular integration

Singular stress around crack tip: $\sigma = f(1/\sqrt{r}, \theta)$

Refinement x 1

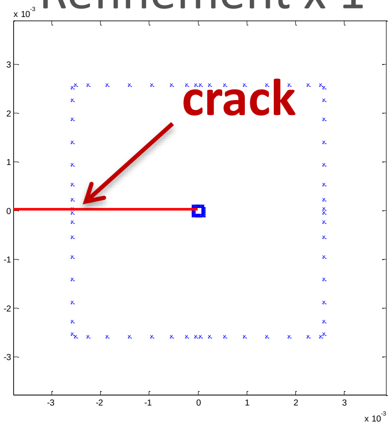

Refinement x 4

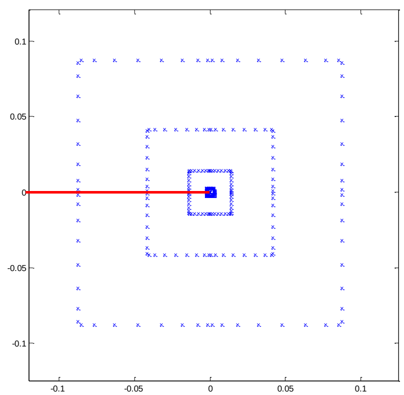

Refinement x 8

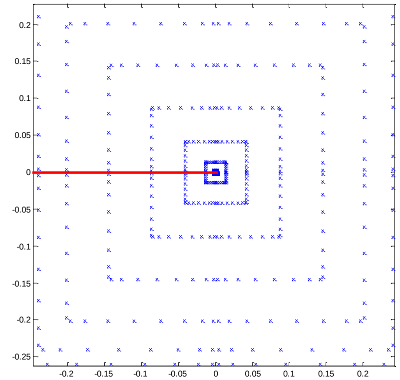

Refinement x 16

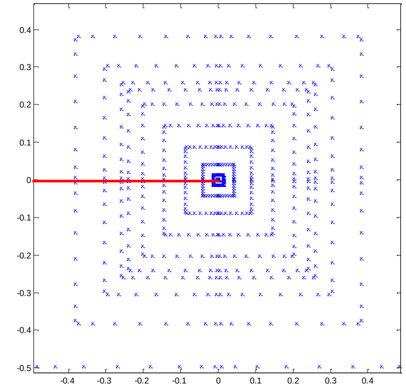

Refinement x 32

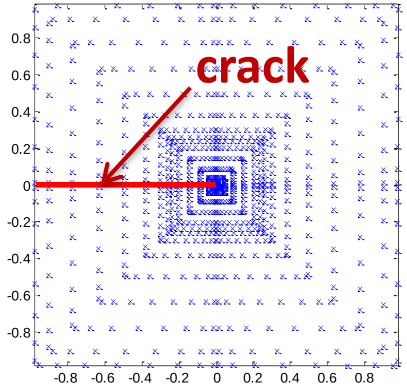

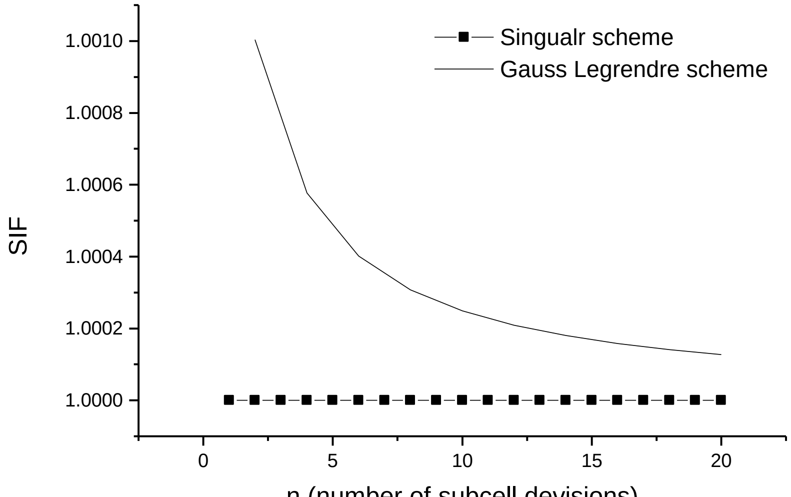

Zhuang, Augarde, Mathisen. International Journal for Numerical Methods in Engineering, Fracture modelling using meshless methods and level sets in 3D: framework and modelling, 92:969-998, 2012.

Meshfree approximation (NOT interpolation)

My contributions:

-Crack representation in 3D based on level sets

-Efficient integration strategy at the crack front

-Evaluation of the interaction integral in 3D

Curvilinear coordinates and level sets for curved crack front and non-planar surface

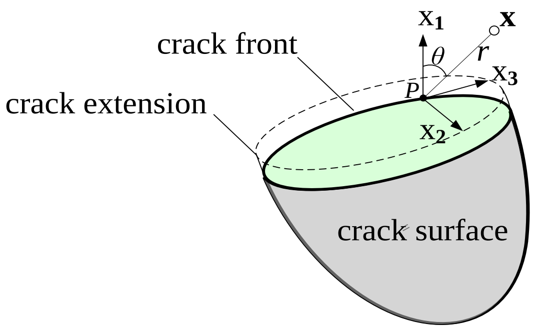

Non-planar crack

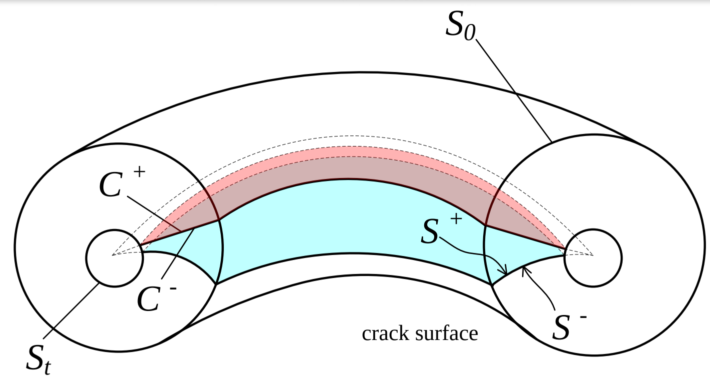

Domain integration along crack front

Energy release over curved crack front domain for non-planar crack

$$\bar{I} = \int_{\Omega} (P_{lj,j} q_l + P_{lj} q_{l,j}) \mathrm{d}\Omega + \int_{C^+ + C^-} P_{lj} q_l n_j \mathrm{d}S + \int_{S^+ + S^-} P_{lj} q_l n_j \mathrm{d}S ,$$

Interaction integral form of Eshelby energy momentum tensor in curvilinear coordinates

$$P_{lj} = \left(\sigma_{ik} \varepsilon_{ik}^{\mathrm{aux}} \delta_{ij} - u_{i,l}^{\mathrm{aux}} \sigma_{ij} - u_{i,l} \sigma_{ij}^{\mathrm{aux}} \right) ,$$

$$u_{1,1} \mathbf{e}_1 \otimes \mathbf{e}_1 \otimes \mathbf{e}_1 \frac{1}{h_1} \frac{\partial}{\partial \xi_1} = u_{1,11} \mathbf{e}_1 \otimes \mathbf{e}_1 \otimes \mathbf{e}_1$$

$$u_{1,1} \mathbf{e}_1 \otimes \mathbf{e}_1 \otimes \mathbf{e}_2 \frac{1}{h_2} \frac{\partial}{\partial \xi_2} = u_{1,12} \mathbf{e}_1 \otimes \mathbf{e}_1 \otimes \mathbf{e}_2$$

$$u_{1,1} \mathbf{e}_1 \otimes \mathbf{e}_1 \otimes \mathbf{e}_3 \frac{1}{h_3} \frac{\partial}{\partial \xi_3} = \frac{h_{3,1}}{h_3} u_{1,1} \mathbf{e}_3 \otimes \mathbf{e}_1 \otimes \mathbf{e}_3 + \frac{h_{3,1}}{h_3} u_{1,1} \mathbf{e}_1 \otimes \mathbf{e}_3 \otimes \mathbf{e}_3$$

$$\frac{h_{3,1}}{h_3} u_1 \mathbf{e}_3 \otimes \mathbf{e}_3 \otimes \mathbf{e}_1 \frac{1}{h_1} \frac{\partial}{\partial \xi_1} = -\frac{h_{3,1}^2}{h_3^2} u_1 \mathbf{e}_3 \otimes \mathbf{e}_3 \otimes \mathbf{e}_1 + \frac{h_{3,1}}{h_3} u_{1,1} \mathbf{e}_3 \otimes \mathbf{e}_3 \otimes \mathbf{e}_1$$

$$\frac{h_{3,1}}{h_3} u_1 \mathbf{e}_3 \otimes \mathbf{e}_3 \otimes \mathbf{e}_2 \frac{1}{h_2} \frac{\partial}{\partial \xi_2} = -\frac{h_{3,1} h_{3,2}}{h_3^2} u_1 \mathbf{e}_3 \otimes \mathbf{e}_3 \otimes \mathbf{e}_2 + \frac{h_{3,1}}{h_3} u_{1,2} \mathbf{e}_3 \otimes \mathbf{e}_3 \otimes \mathbf{e}_2$$

$$\frac{h_{3,1}}{h_3} u_1 \mathbf{e}_3 \otimes \mathbf{e}_3 \otimes \mathbf{e}_3 \frac{1}{h_3} \frac{\partial}{\partial \xi_3} = -\frac{h_{3,1}^2}{h_3^2} u_1 \mathbf{e}_1 \otimes \mathbf{e}_3 \otimes \mathbf{e}_3 - \frac{h_{3,1} h_{3,2}}{h_3^2} u_1 \mathbf{e}_2 \otimes \mathbf{e}_3 \otimes \mathbf{e}_3 - \frac{h_{3,1}^2}{h_3^2} u_1 \mathbf{e}_3 \otimes \mathbf{e}_1 \otimes \mathbf{e}_3 - \frac{h_{3,1} h_{3,2}}{h_3^2} u_1 \mathbf{e}_3 \otimes \mathbf{e}_2 \otimes \mathbf{e}_3$$

Zhuang, Augarde, Mathisen. International Journal for Numerical Methods in Engineering, Fracture modelling using meshless methods and level sets in 3D: framework and modelling, 92:969-998, 2012.

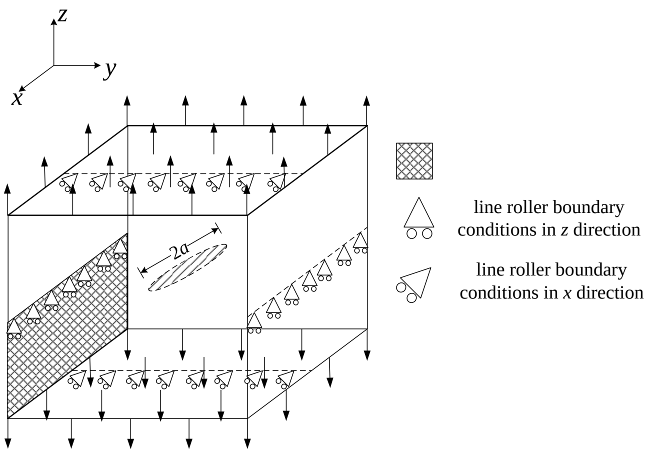

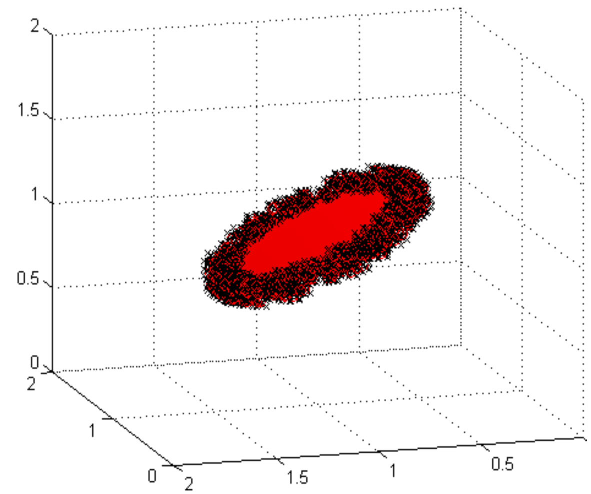

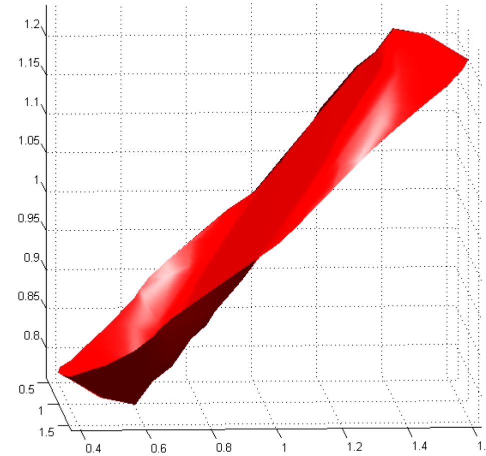

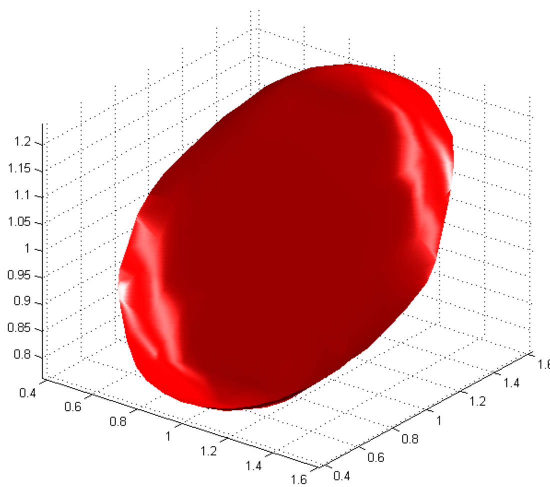

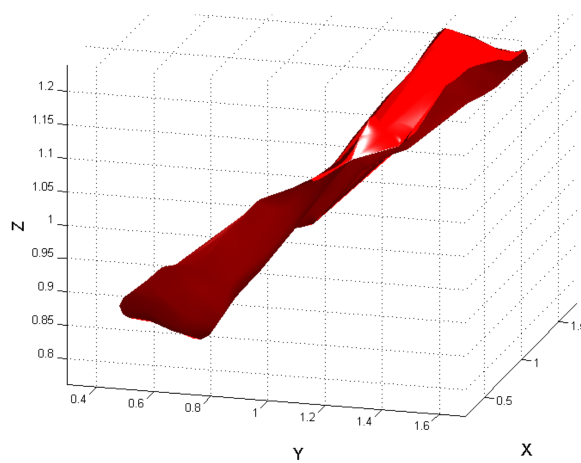

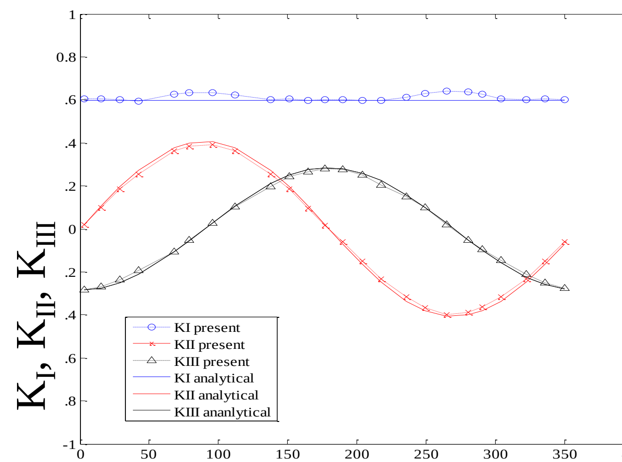

SIF results along crack front θ °

Zhuang, Augarde, Mathisen. International Journal for Numerical Methods in Engineering, Fracture modelling using meshless methods and level sets in 3D: framework and modelling, 92:969-998, 2012.

Meshfree methods and particle methods
Discontinuous deformation analysis for blocky system

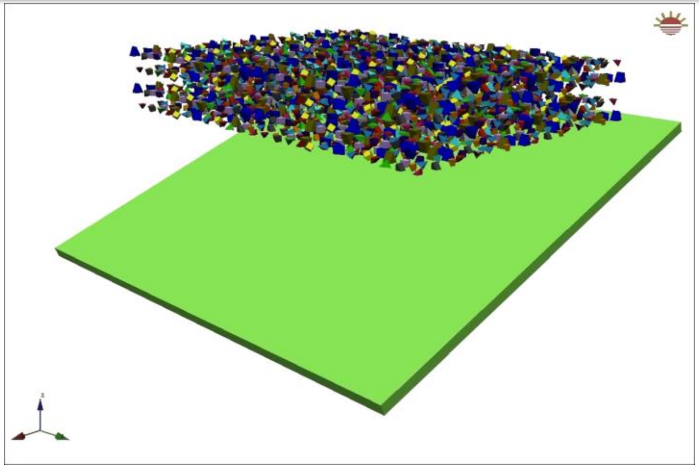

3D DDA model of particle flow

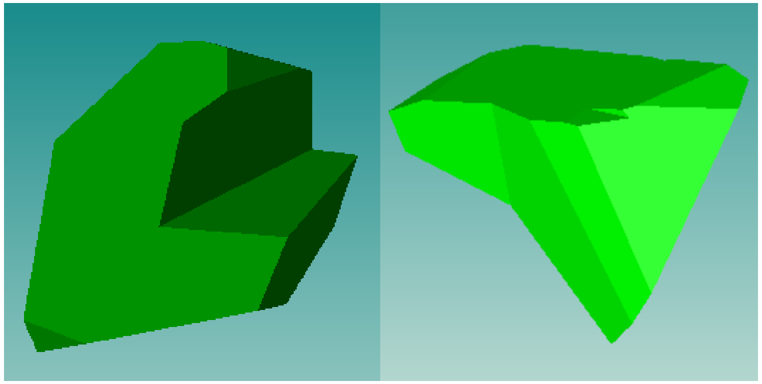

Concave blocks

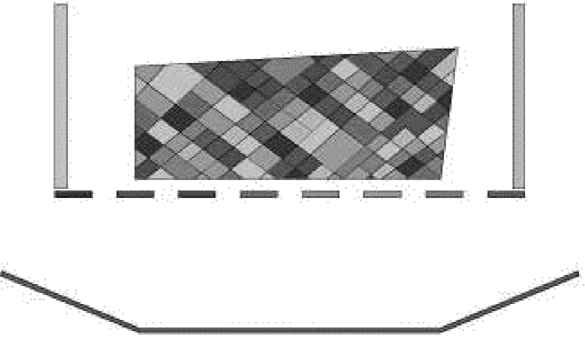

0.05Hz

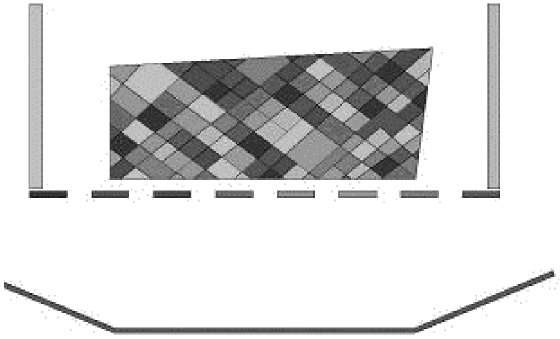

0.25Hz

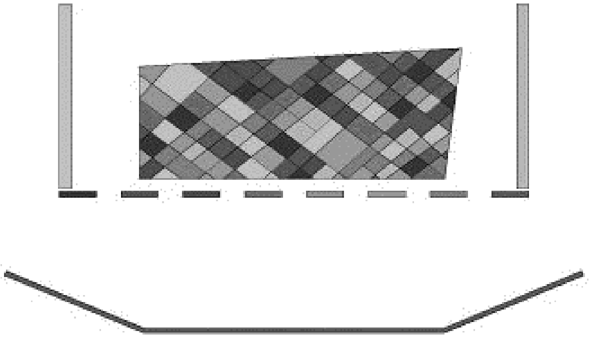

1.0Hz

Vibrating screen with different frequency

Zhu, Wu, Zhuang, Cai. Method for estimating normal contact parameters in collision modeling using discontinuous deformation analysis. ASCE International Journal of Geomechanics, paper in press, 2016.

Contact detection is the most expensive part of DDA!

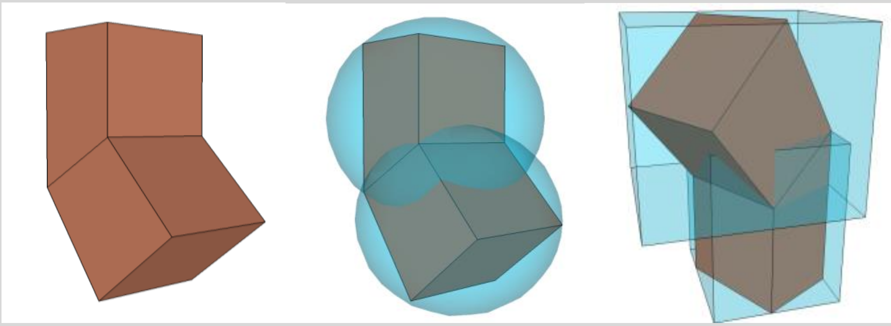

A new multi-shell cover contact detection method

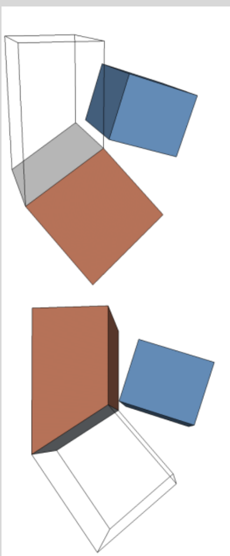

Concave block

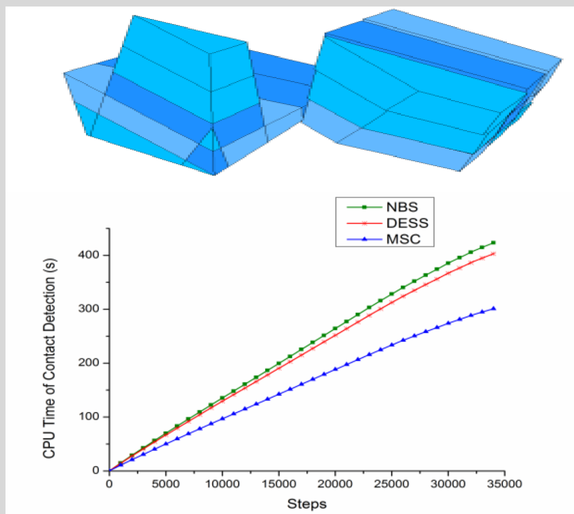

Contact detection efficiency improved by multi-shell cover (MSC)

Common plane method

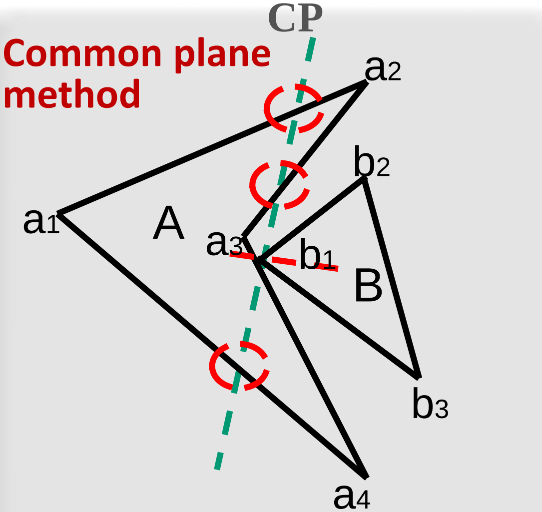

Shortest link method

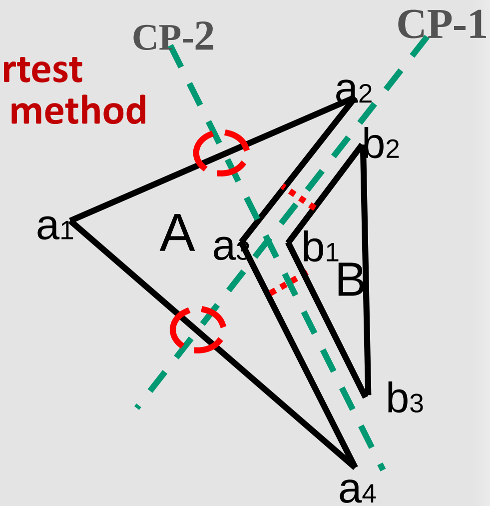

Conventional methods invalid for concave block

Wu, Zhu, Zhuang, Ma, Cai. A multi-shell cover algorithm for contact detection in the three dimensional discontinuous deformation analysis. Theoretical and Applied Fracture Mechanics, 72: 136-149, 2014.

Peridynamics

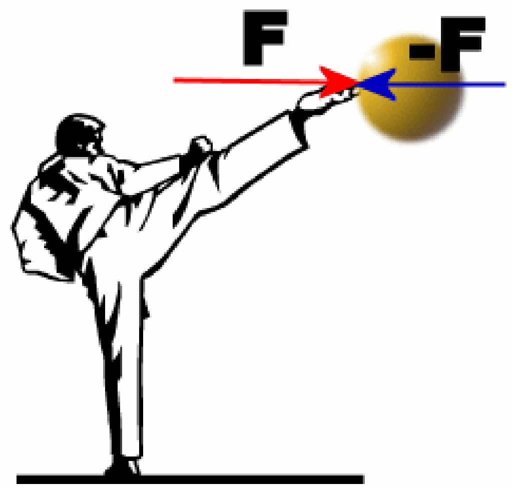

Local model

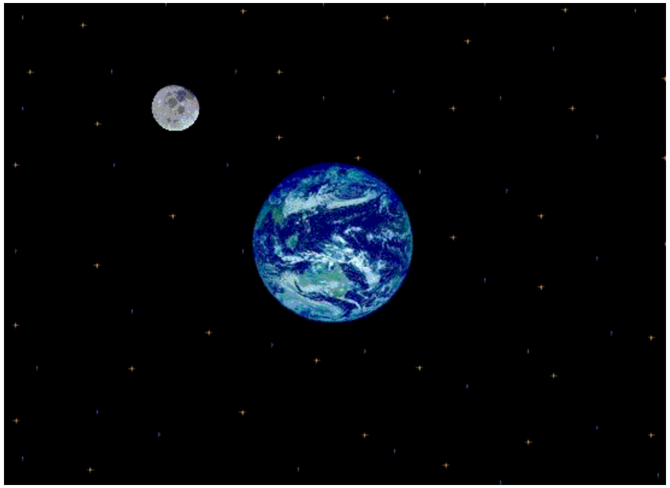

Nonlocal model

Horizon H_x
Domain where any particle falling inside will receive the forces exerted by x

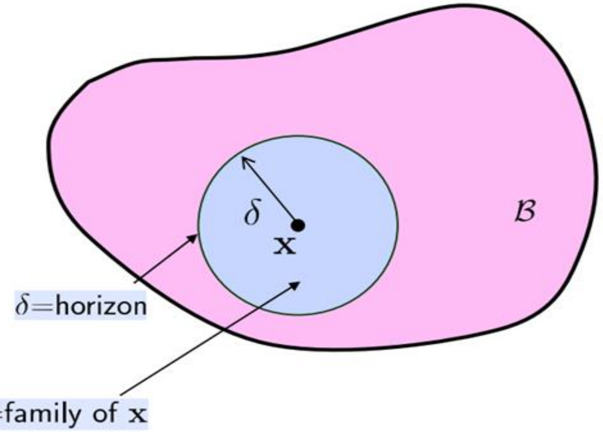

Peridynamics and horizon of particle

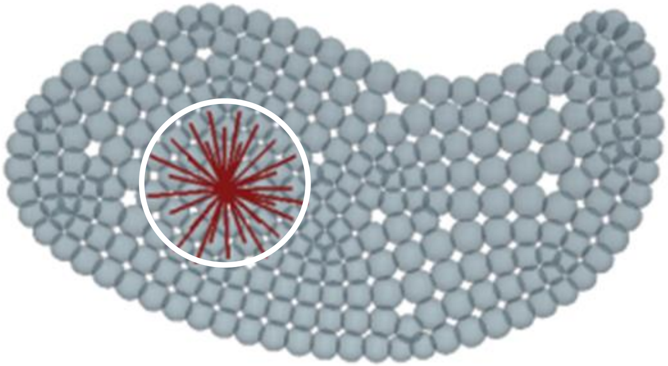

Particles interact each other similar to planets or atoms

Peridynamics

Classical equations of motion has divergence term

$$\rho(\mathbf{x})\ddot{\mathbf{u}}(\mathbf{x},t) = \boxed{\nabla \cdot}\sigma + \mathbf{b}(\mathbf{x},t)$$

Peridynamics uses an integral form rather than differential form

$$\rho(\mathbf{x})\ddot{\mathbf{u}}(\mathbf{x},t) = \int_{H_{\mathbf{x}}} \mathbf{f}(\mathbf{u}(\mathbf{x}',t) - \mathbf{u}(\mathbf{x},t), \mathbf{x}' - \mathbf{x})\, \mathrm{d}V_{\mathbf{x}'} + \mathbf{b}(\mathbf{x},t)$$

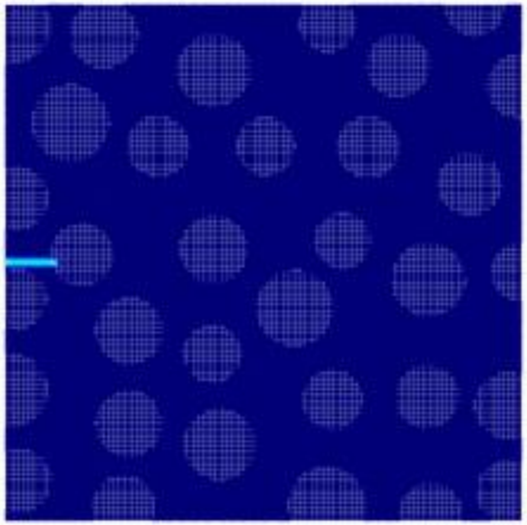

Fractures are the natural outcome!

Crack branching, coalescence…

Silling S.A.: Reformulation of elasticity theory for discontinuities and long-range forces, Journal of the Mechanics and Physics of Solids, **2000**, 48(1): 175-209

Constant horizon constraints in Peridynamics

- Computational cost too expensive when using constant horizon!
- But non-constant horizon sizes results in spurious wave reflection!

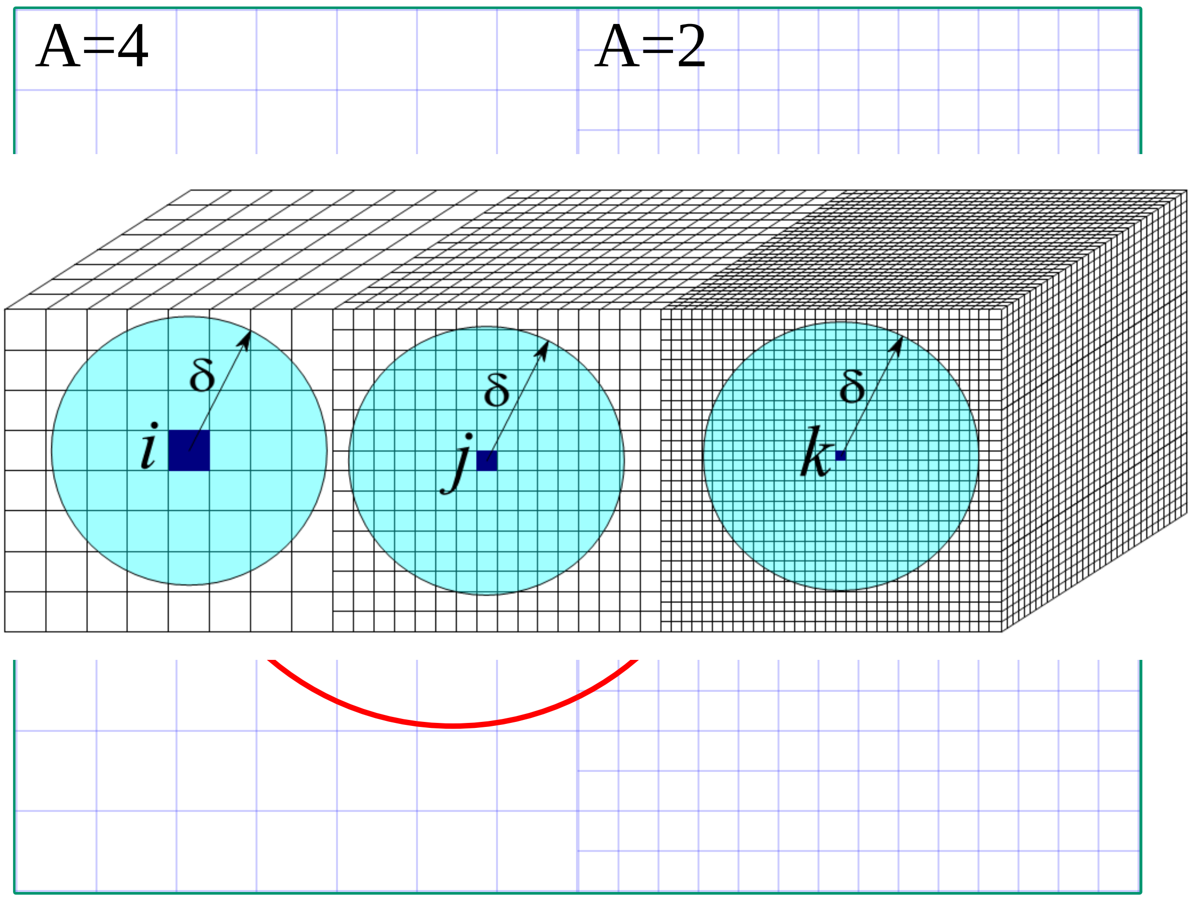

$$\mathbf{x} \notin H_{\mathbf{x}'} \Rightarrow \mathbf{F}_{\mathbf{x}\mathbf{x}'} = 0$$

$$\mathbf{x}' \in H_{\mathbf{x}} \Rightarrow \mathbf{F}_{\mathbf{x}'\mathbf{x}} \neq 0$$

$$\mathbf{F}_{\mathbf{x}\mathbf{x}'} \neq -\mathbf{F}_{\mathbf{x}'\mathbf{x}}$$

Newton's third law violated.
Fundamental Symmetry broken

- Ghost force issue
- Spurious wave reflection

Dual-horizon peridynamics

Horizon H_x
Domain where particle falling inside will receive the forces exerted by x

Dual-Horizon $H'_{\mathbf{x}} = \{\mathbf{x}' | \mathbf{x} \in H_{\mathbf{x}'}\}.$
A union of points whose horizons include x

Inertia force $\rho\ddot{\mathbf{u}}(\mathbf{x}, t)$

Body force $\mathbf{b}(\mathbf{x}, t)$

Direct bond force

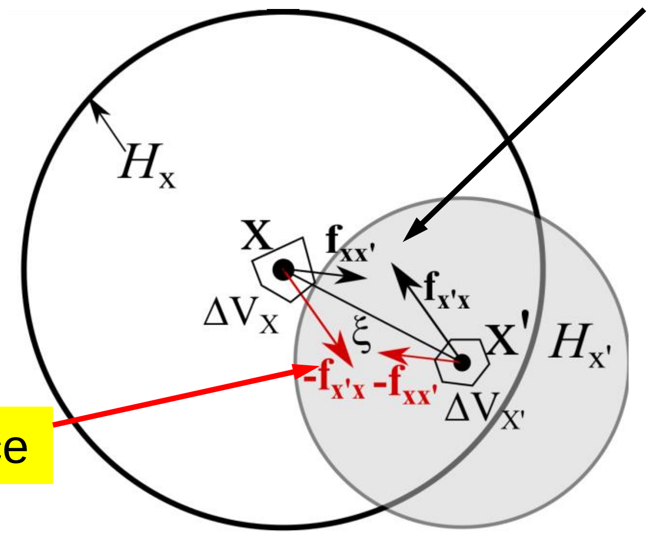

Reaction bond force

Dual-horizon peridynamics

$$\rho\ddot{\mathbf{u}}(\mathbf{x}, t) = \boxed{\int_{\mathbf{x}' \in H'_{\mathbf{x}}} \mathbf{f}_{\mathbf{x}\mathbf{x}'}(\boldsymbol{\eta}, \boldsymbol{\xi})\, \mathrm{d}V_{\mathbf{x}'} - \int_{\mathbf{x}' \in H_{\mathbf{x}}} \mathbf{f}_{\mathbf{x}'\mathbf{x}}(-\boldsymbol{\eta}, -\boldsymbol{\xi})\, \mathrm{d}V_{\mathbf{x}'}} + \mathbf{b}(\mathbf{x}, t)$$

Conventional peridynamics

$$\rho\ddot{\mathbf{u}}(\mathbf{x}, t) = \boxed{\int_{H_{\mathbf{x}}} [\mathbf{f}_{\mathbf{x}\mathbf{x}'}(\boldsymbol{\eta}, \boldsymbol{\xi}) - \mathbf{f}_{\mathbf{x}'\mathbf{x}}(-\boldsymbol{\eta}, -\boldsymbol{\xi})]\mathrm{d}V_{\mathbf{x}'}} + \mathbf{b}(\mathbf{x}, t) \ ,$$

Ren H., Zhuang X., Cai Y., Rabczuk T..: Dual Horizon Peridynamics, International Journal for Numerical Methods in Engineering, DOI: 10.1002/nme.5257, 2016.

Dual-horizon peridynamics
Variable horizon sizes without any spurious force issue

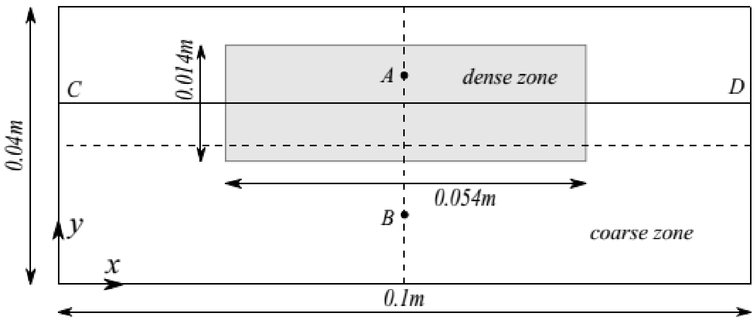

Wave propagation of plate

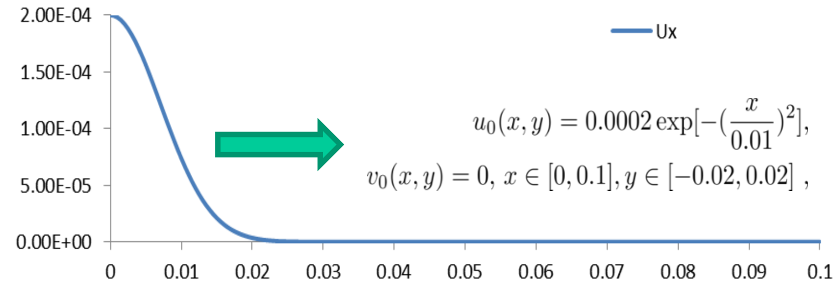

Initial displacement profile

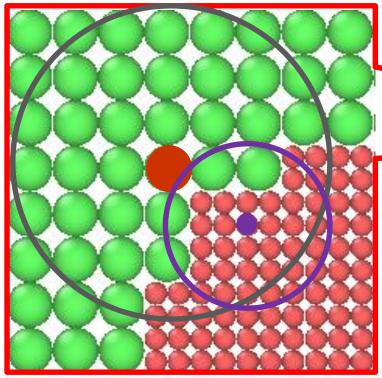

Variable horizon sizes

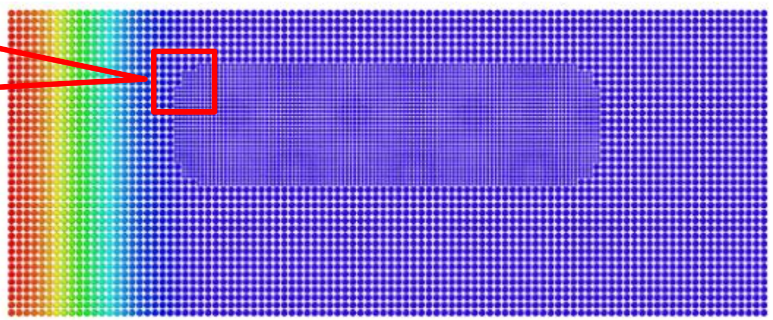

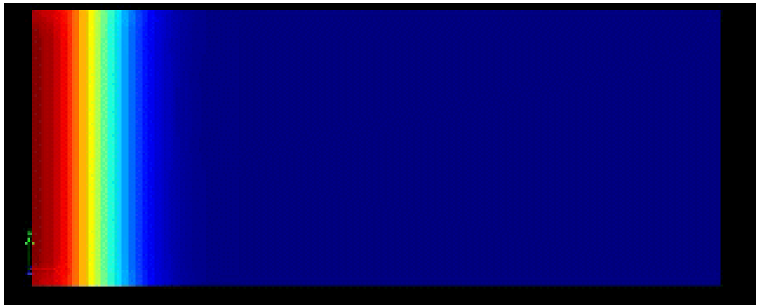

Dual-horizon peridynamics

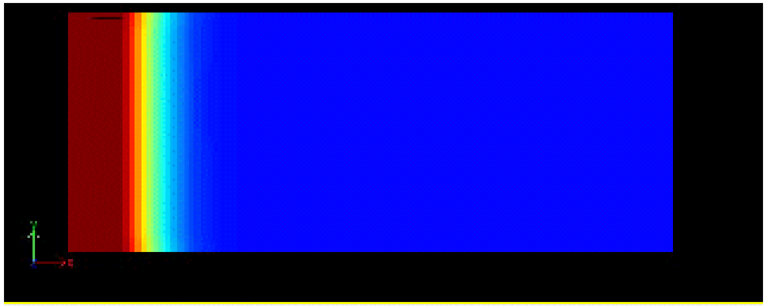

Conventional peridynamics

Dual-horizon peridynamics
Variable horizon sizes without any spurious force issue

L_2 error norm comparison

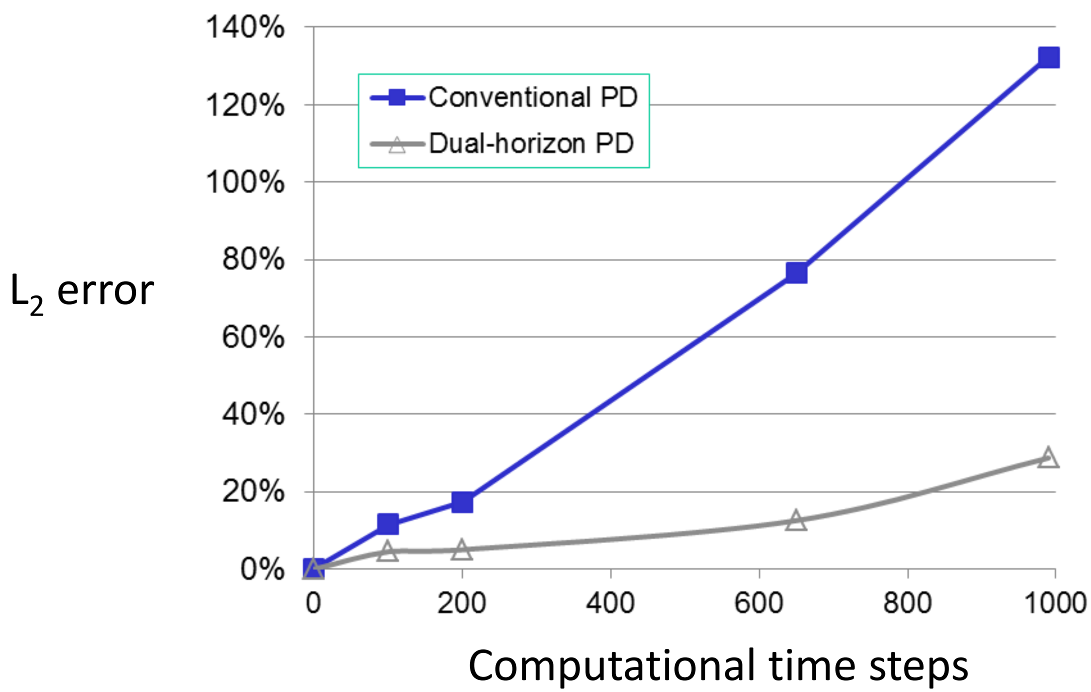

$$\|\mathrm{err}\|_{L_2} = \frac{\|\mathbf{u}^h - \mathbf{u}_{\mathrm{analytic}}\|}{\|\mathbf{u}_{\mathrm{analytic}}\|}\ , \ \text{where } \|\mathbf{u}\| = \left(\int_{\Omega_0} \mathbf{u}\cdot\mathbf{u}\, d\Omega_0\right)^{\frac{1}{2}}\ .$$

Ren H., Zhuang X., Cai Y., Rabczuk T..: Dual Horizon Peridynamics, International Journal for Numerical Methods in Engineering, DOI: 10.1002/nme.5257, 2016.

Dual-horizon peridynamics
Stable results with varying horizon sizes

Kalthoff-Winkler Experiments

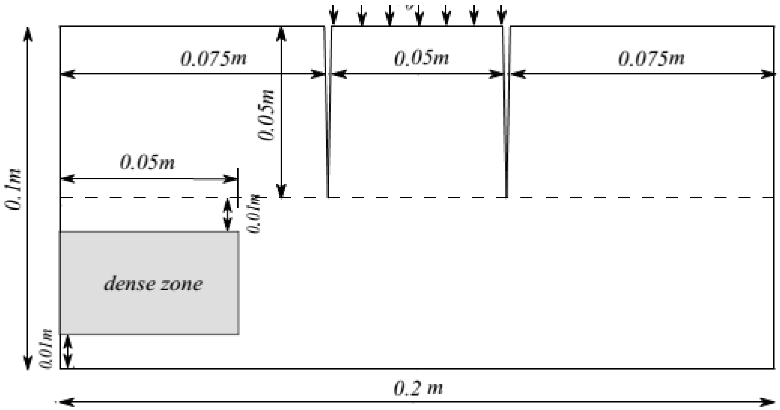

Parameter	value
Density	7800 kg/m^3
Elastic modulus	190 Gpa
Poisson ratio	0.25
G_0	6.9e4 J/m^2
Impact velocity	22m/s
Thickness	0.01m
Total particles	57968

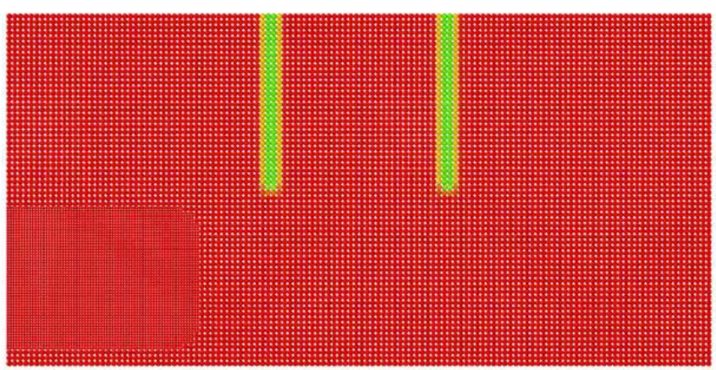

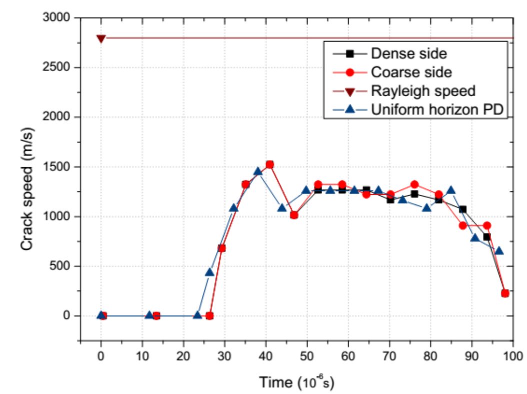

Ren H., Zhuang X., Cai Y., Rabczuk T..: Dual Horizon Peridynamics, International Journal for Numerical Methods in Engineering, DOI: 10.1002/nme.5257, 2016.

Dual-horizon peridynamics
Stable results with varying horizon sizes

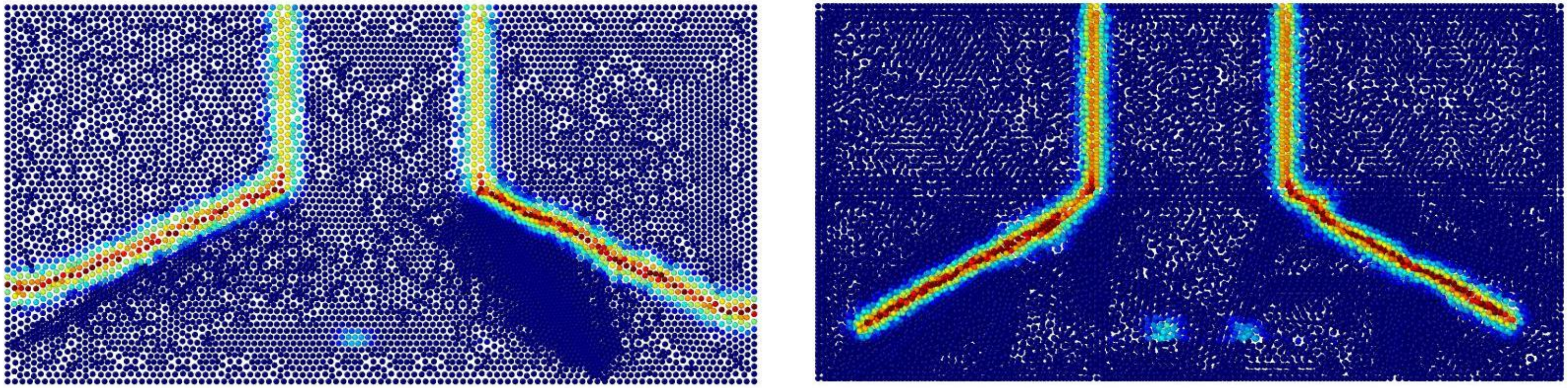

Dual-horizon peridynamics

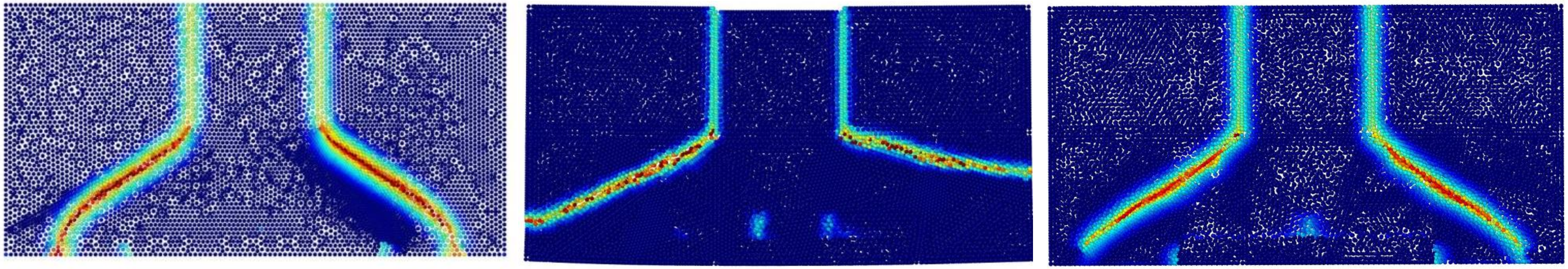

Conventional peridynamics

Adaptive refinement along crack paths

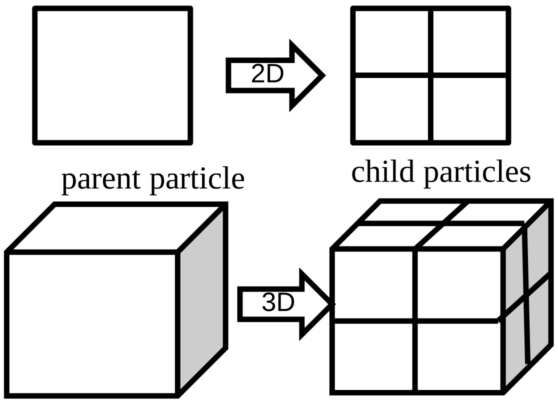

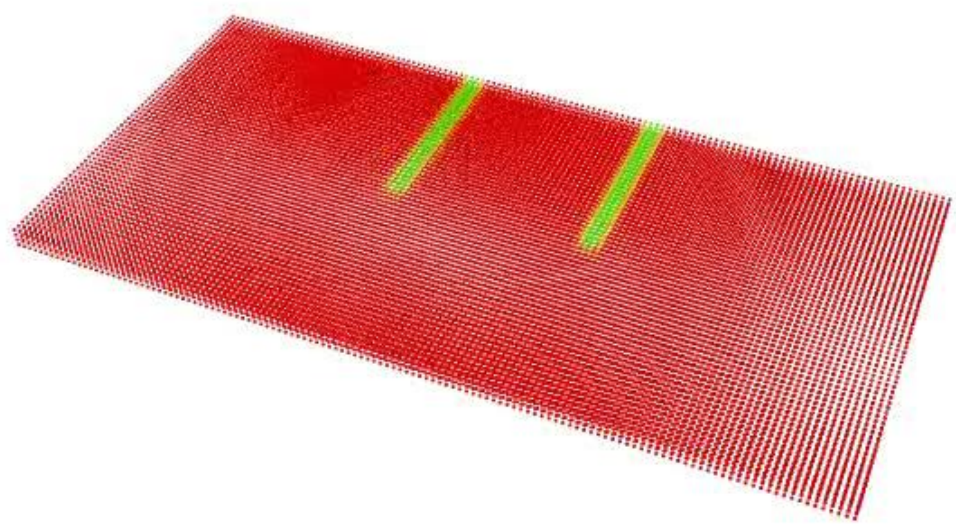

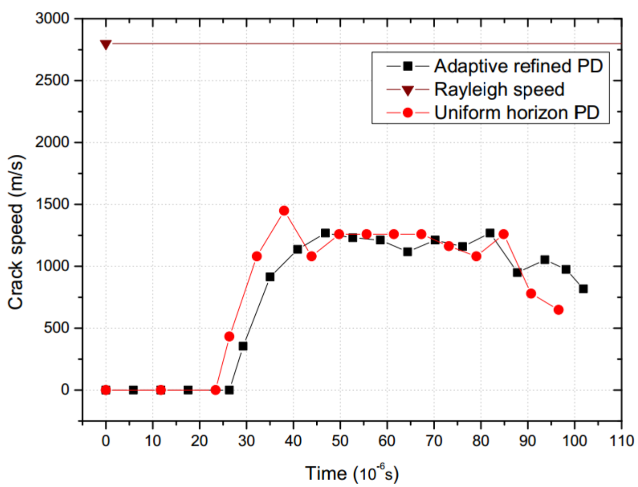

Ren H., Zhuang X., Cai Y., Rabczuk T..: Dual Horizon Peridynamics, International Journal for Numerical Methods in Engineering, DOI: 10.1002/nme.5257, 2016.

Dual-horizon peridynamics
Adaptive refinement

Plate with pre-crack subjected to traction

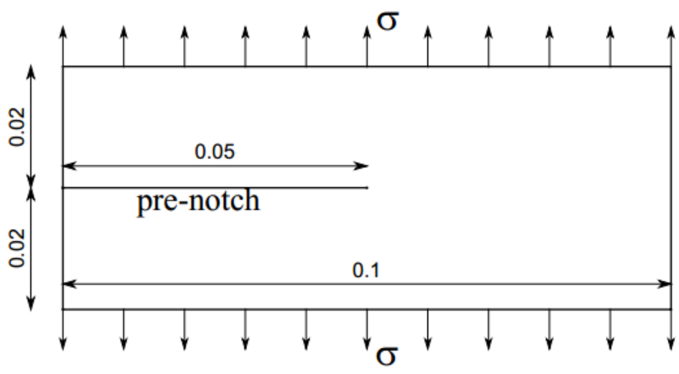

Parameter	value
Density	2440 kg/m^3
Elastic modulus	72 GPa
Poisson ratio	0.33
G_0	135 J/m^2
Traction stress	22 MPa
Thickness	0.01m
Total particles	4000-6424

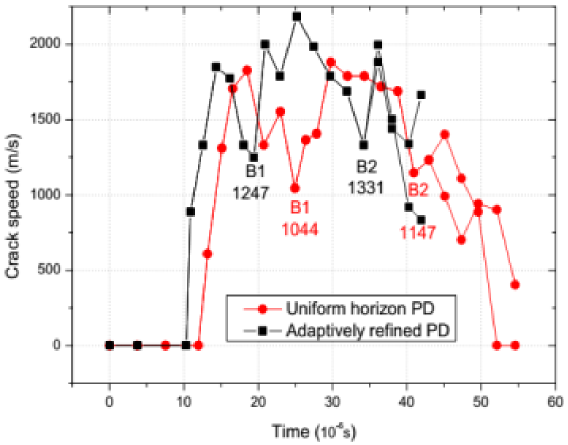

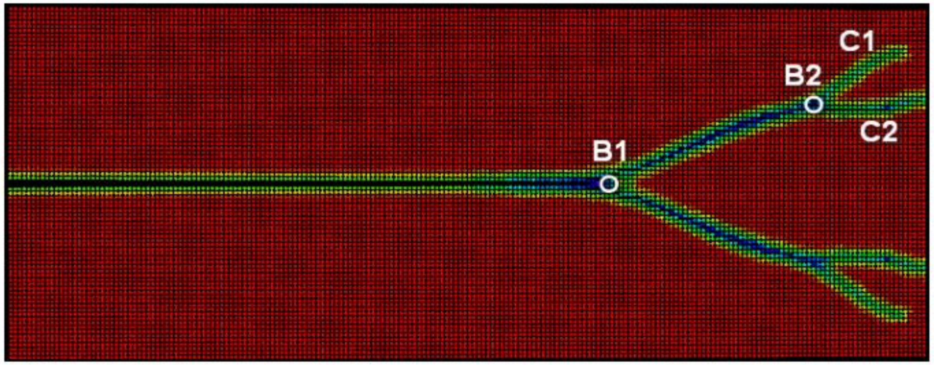

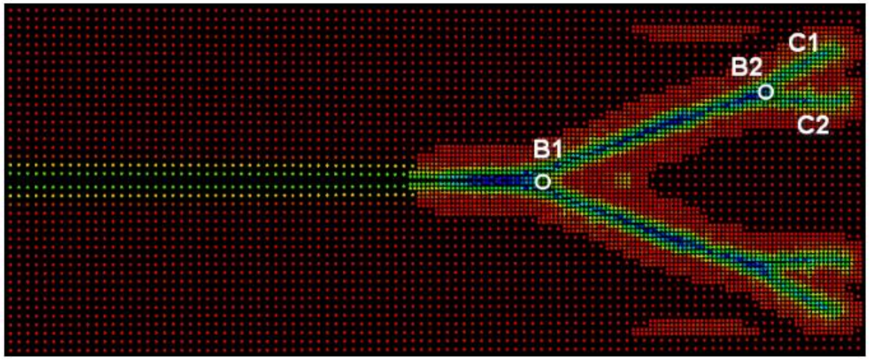

Ren H., Zhuang X., Cai Y., Rabczuk T..: Dual Horizon Peridynamics, International Journal for Numerical Methods in Engineering, DOI: 10.1002/nme.5257, 2016.

Overview

- Computational Methods for Fracture
    - Meshfree and Particle Methods
    - Peridynamics
- Application to the design of polymer-matrix composites
    - Framework
    - Models at different length scales
    - Multiscale approach
    - Sensitivity analysis and optimisation

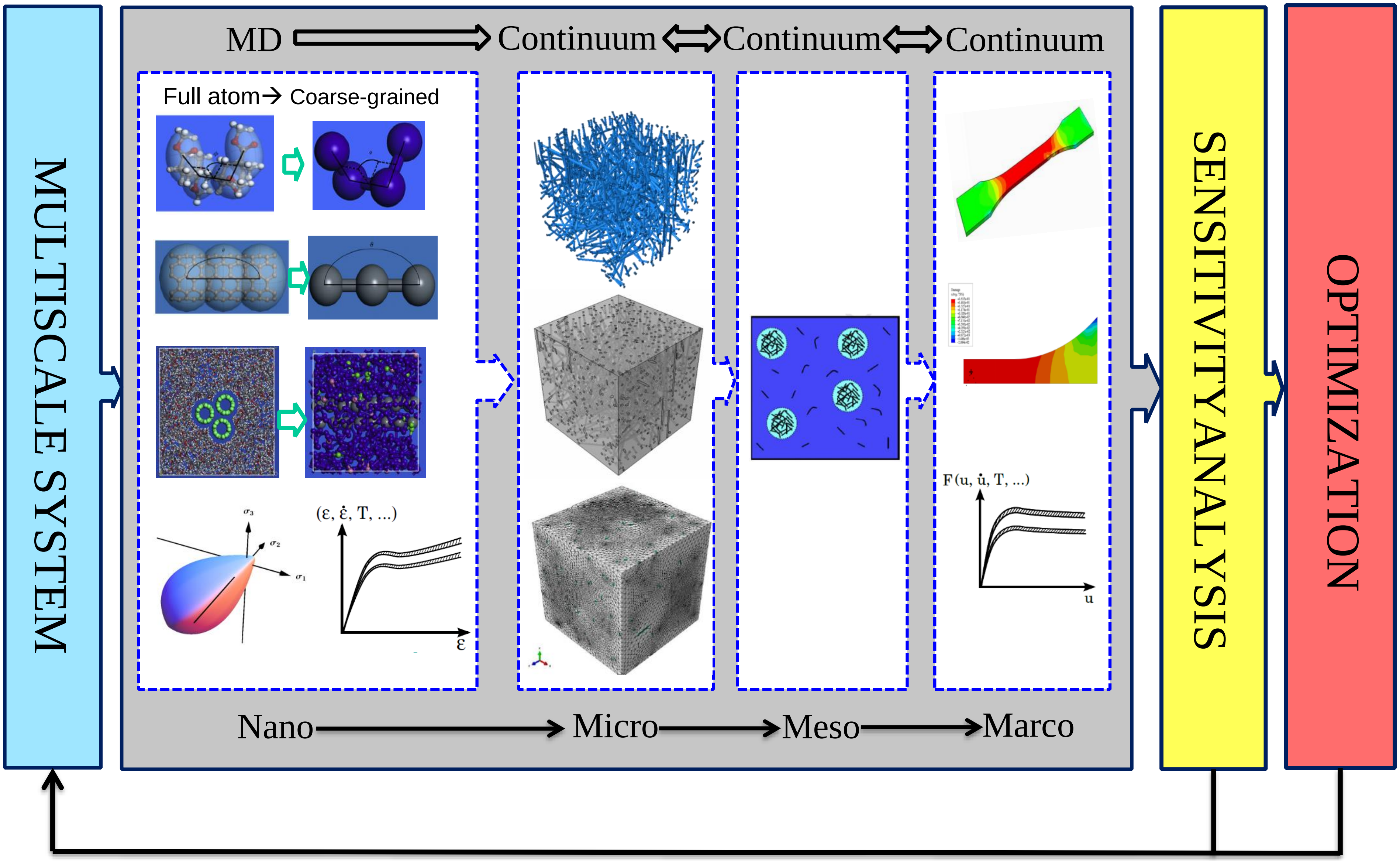
MULTISCALE SYSTEM
MD
Continuum
Continuum
Continuum
Full atom
Coarse-grained
(ε, ε̇, T, ...)
ε
F(u, u̇, T, ...)
u
Nano
Micro
Meso
Marco
SENSITIVITY ANALYSIS
OPTIMIZATION

Sofja Kovalevskaja Programme

von Humboldt
Stiftung / Found

- Topic: Computational Characterization, Testing and Design of Carbon Fiber Based Polymer Matrix Composites
- Budget: 1.65 M Euros
- Duration: Dec 2015 – Nov 2020

Group members

Postdocs

PhD students

Nanthakumar Subbiah

Shuai Zhou
周帅

Yiming Zhang
张一鸣

Binh Nguyen Huy

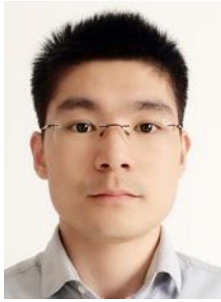

Bo He
何博

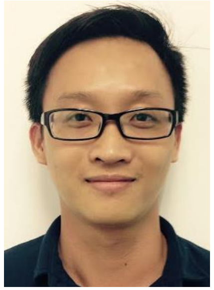

Minh

Thai

Overview

- Computational Methods for Fracture
  - Meshfree and Particle Methods
  - Peridynamics
- Application to the design of polymer-matrix composites
  - Framework
  - Models at different length scales
  - Multiscale approach
  - Sensitivity analysis and optimisation

Coarse-grained model for CNT/polymer

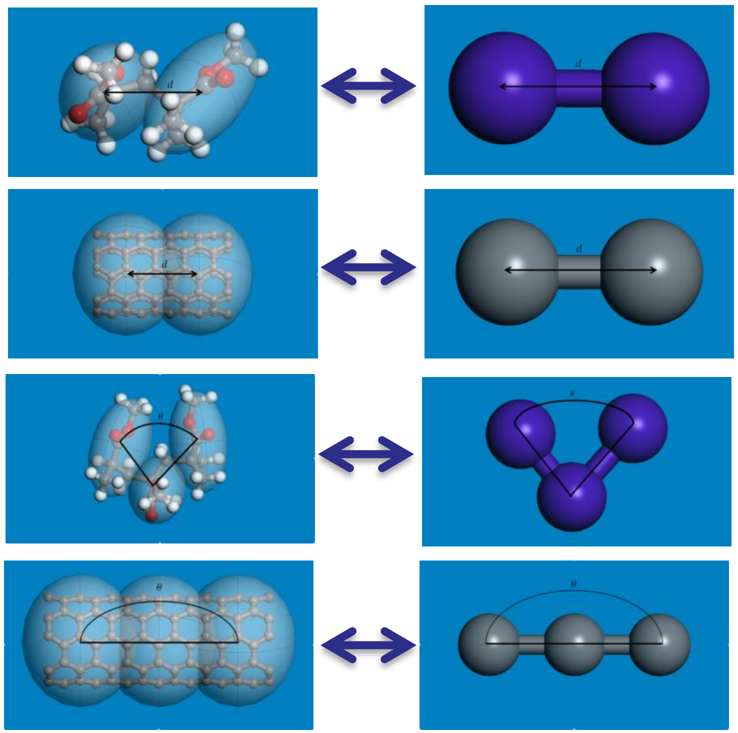

Atomistic model versus coarse-grained model

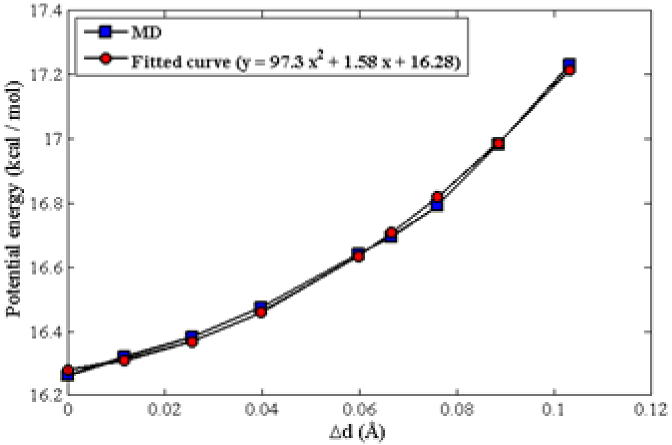

Parametrization of CG force fields.

$$E_b(d) = \frac{k_d}{2}(d - d_0)^2$$

$$E_a(\theta) = \frac{k_\theta}{2}(\theta - \theta_0)^2$$

$$E_d(\phi) = \frac{k_\phi}{2}[1 + \cos 2\phi]$$

$$U_{total} = \sum_i E_{b_i} + \sum_j E_{a_j} + \sum_k E_{d_k} + \sum_{lm} E_{vdW_{lm}} + U_0$$

$$E_{vdW}(r) = D_0\left[\left(\frac{r_0}{r}\right)^{12} - 2\left(\frac{r_0}{r}\right)^{6}\right]$$

A.A. Mousavi, B. Arash, X. Zhuang, T. Rabczuk. A coarse-grained model for the elastic properties of cross linked short carbon nanotube/polymer composites, Composites Part B, 2015.

Coarse-grained model for CNT/polymer

CG model Illustrations of $2CH_2$ **cross link** between a PMMA monomer and a CNT resulting from atomistic models.

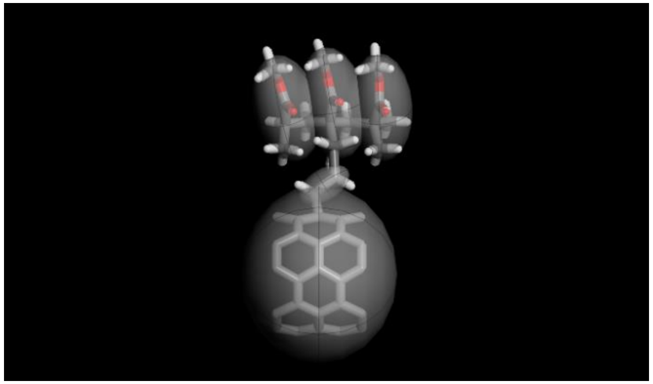

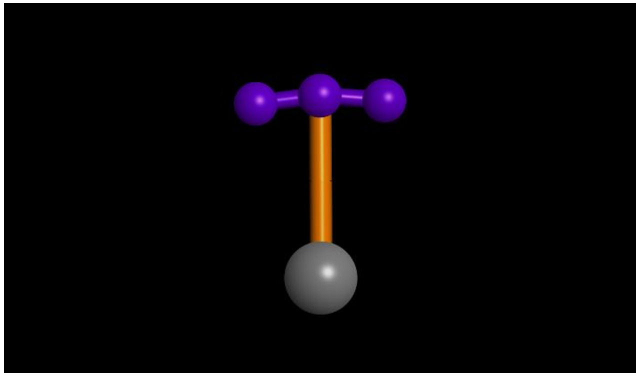

The spring constant is $142.71(\frac{kcal}{mol}/\overset{\circ}{A}{}^2)$. The equilibrium distance between two beads is $9.487(\overset{\circ}{A})$

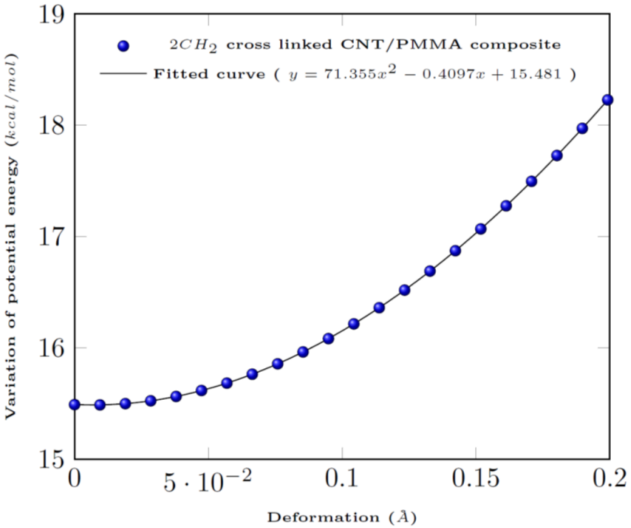

Coarse-grained model for CNT/polymer

EGDMA **cross link between two PMMA monomers**

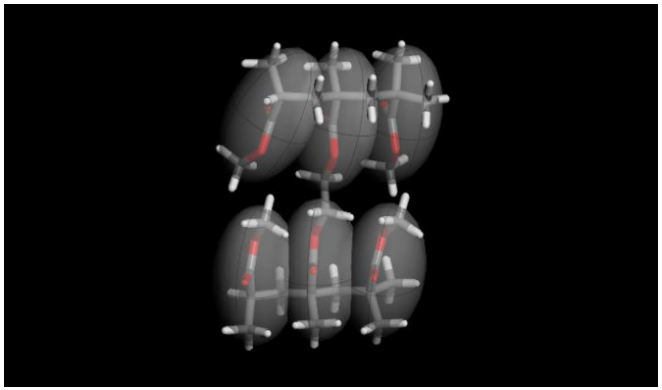

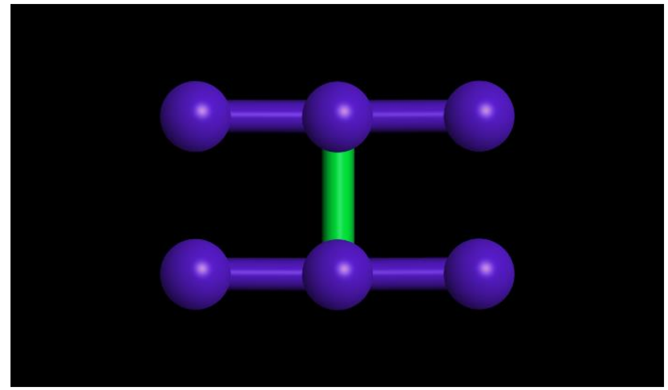

The spring constant is 150.206($\frac{kcal}{mol}/A^{\circ 2}$). The equilibrium distance between two beads is 6.21(A°)

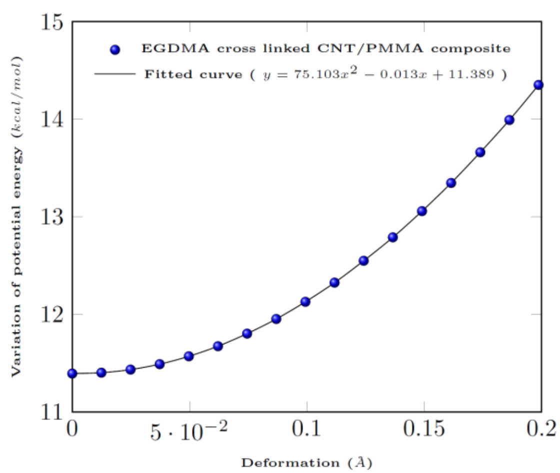

Coarse-grained model for CNT/polymer

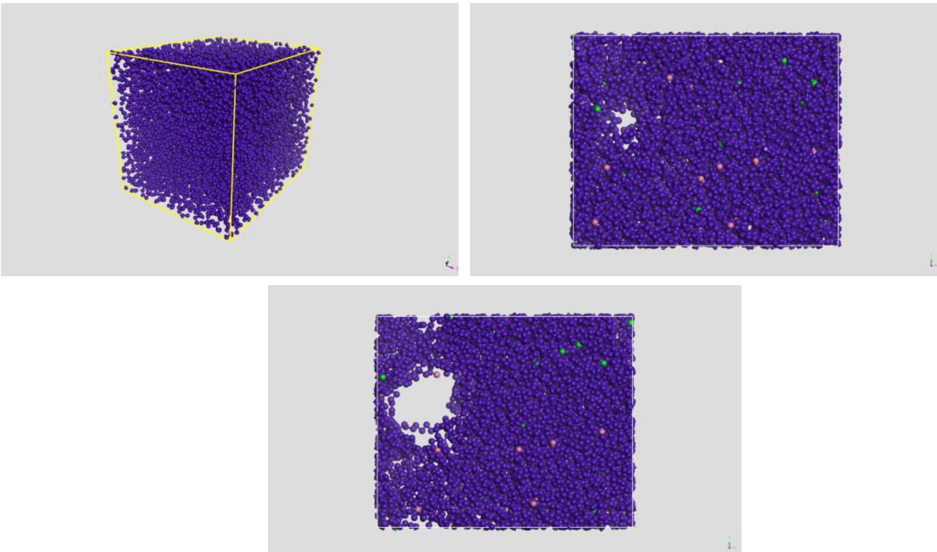

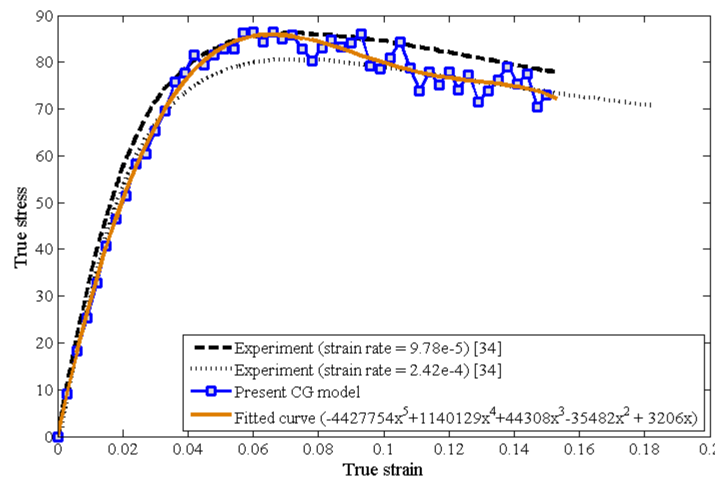

Tensile fracture of a pure PMMA polymer.

	Experiment (Strain rate=2.42e-4)	Experiment (Strain rate=9.87e-5)	Present CG model
Young’s modulus (GPa)	3.27	3.12	2.88
Yield strength (MPa)	56.6	51.4	52.30
Tensile strength (MPa)	86.9	79.6	85.82
Critical strain	0.165	0.178	0.159

Coarse-grained model for CNT/polymer

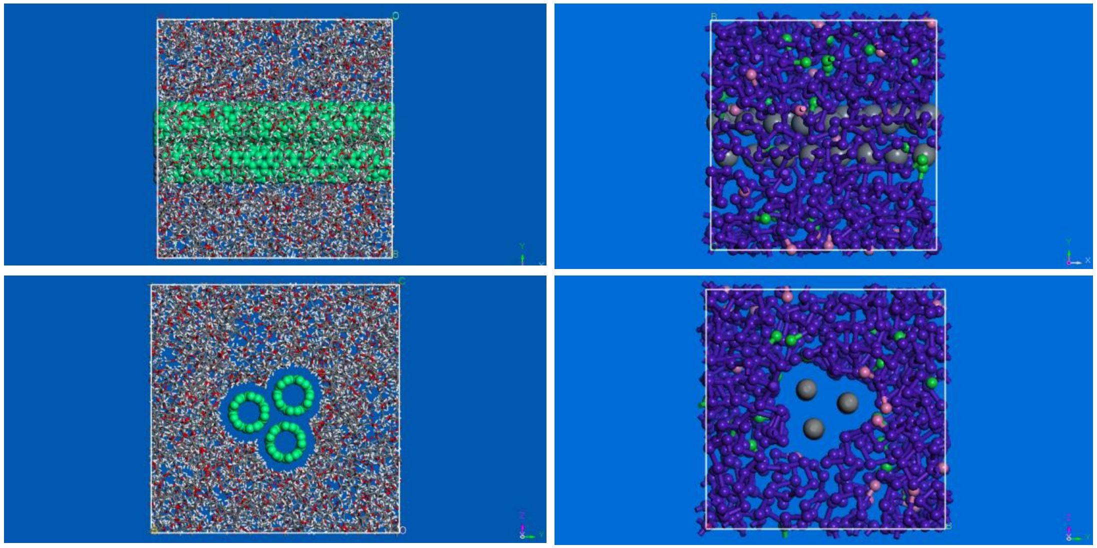

Atomistic and coarse-grained RVE of a CNT/PMMA composite.

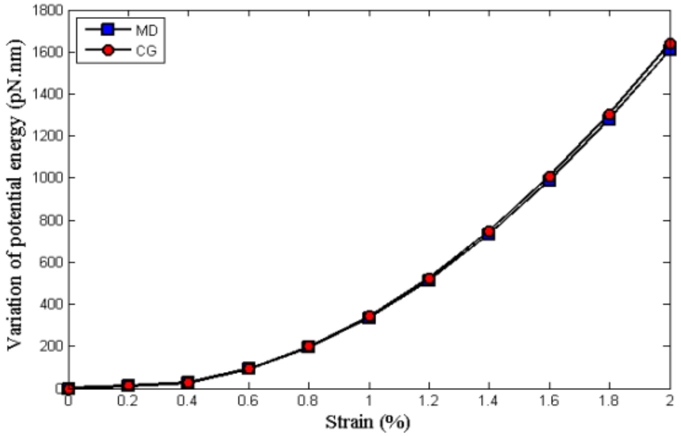

Variation of potential energy of the composite versus strain

Volume fraction of CNTs (%)	CG (GPa)	MD (GPa)
10 (3 CNTs)	73.39	72.54
13.38 (4 CNTs)	97.13	96.05
16.73 (5 CNTs)	122.05	121.30
20 (6 CNTs)	145.49	145.34

Coarse-grained model for CNT/polymer

Tensile strength w.r.t. fiber length and wt%

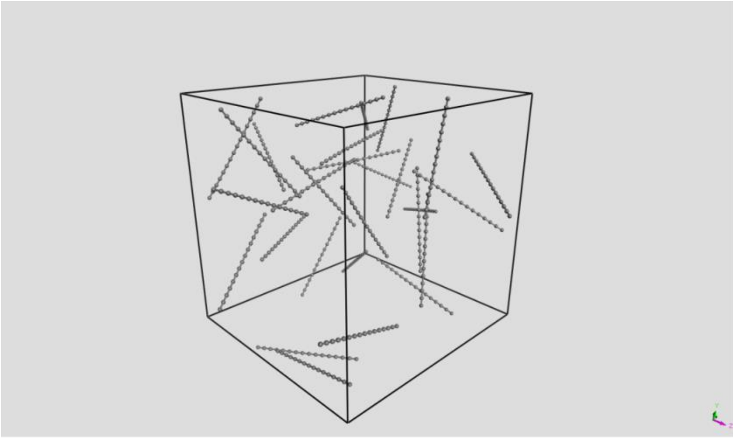

Tensile strength of CNT/PMMA composites

wt (%)	Young's modulus (GPa)	Tensile strength (MPa)
5	3.05	92.44
8	3.11	94.80
10	3.24	99.63

L/D	Young's modulus (GPa)	Tensile strength (MPa)
14.7	3.11	94.80
29.4	3.59	101.82
44.1	4.01	111.61

Crack propagation of two-phase composites

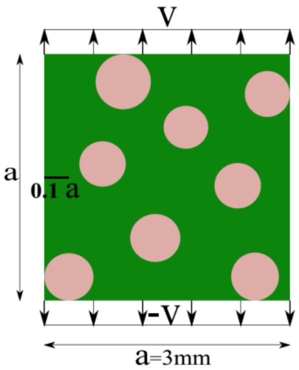

Boundary condition v=0.5 m/s

Critical stretch is $s_0(\delta) = \sqrt{\dfrac{4\pi G_0}{9E\delta}}$

Type	E (Gpa)	Poisson's ratio	G_0 (J/m2)
Matrix	72	1/3	40
Reinformcement	144	1/3	80

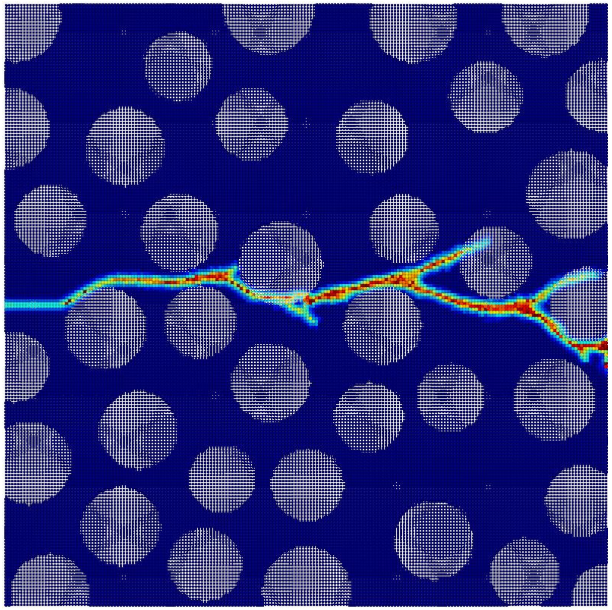

Case 1: v=0.5m/s

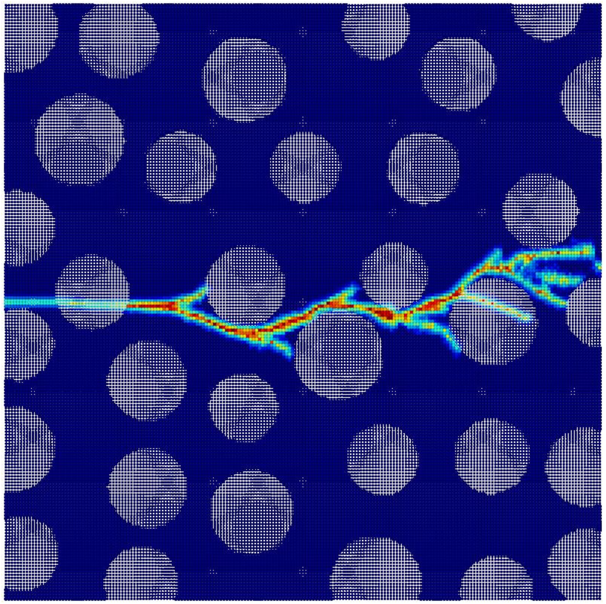

Case 2: v=0.5m/s

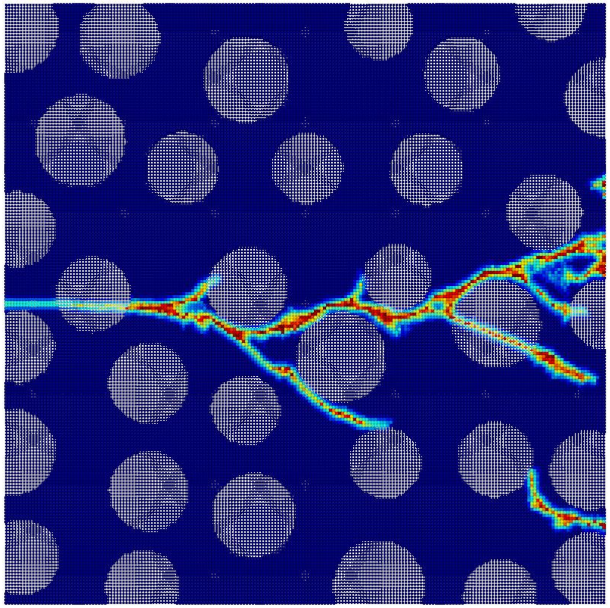

Case 3: v=2m/s

Crack propagation of two-phase composites

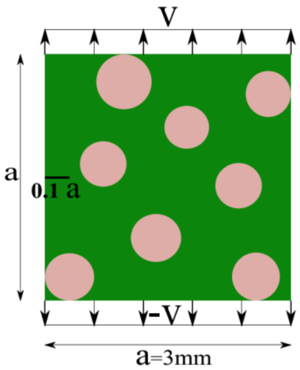

Boundary condition v=0.5 m/s

Critical stretch is $s_0(\delta) = \sqrt{\dfrac{4\pi G_0}{9E\delta}}$

Type	E (Gpa)	Poisson's ratio	G_0 (J/m2)
Matrix	72	1/3	40
Reinformcement	144	1/3	80

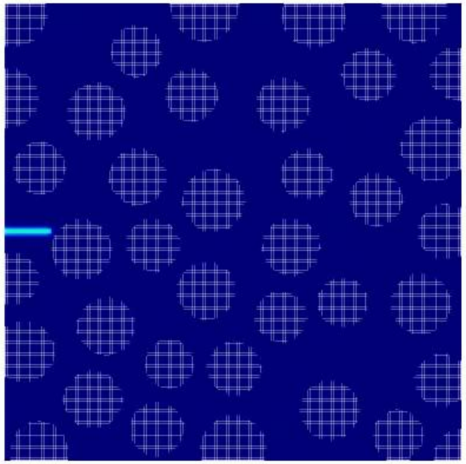

Case 1: v=0.5m/s

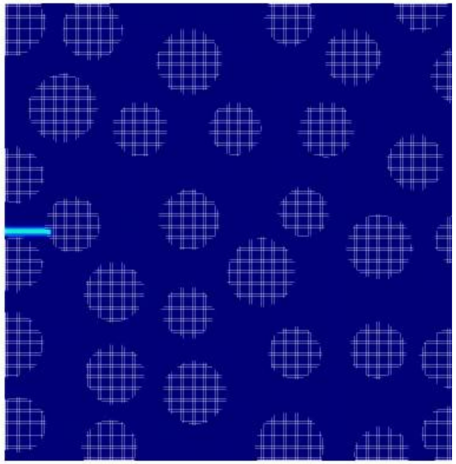

Case 2: v=0.5m/s

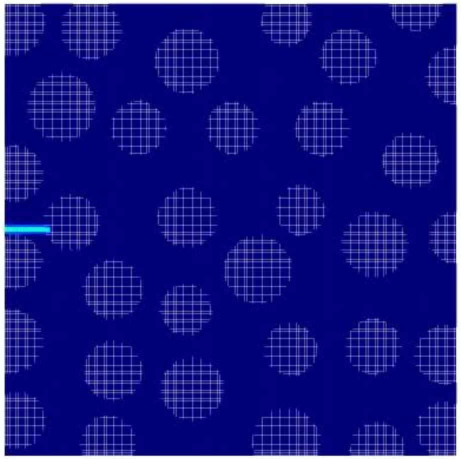

Case 3: v=2m/s

Overview

- Computational Methods for Fracture
  - Meshfree and Particle Methods
  - Peridynamics
- Application to the design of polymer-matrix composites
  - Framework
  - Models at different length scales
  - Multiscale approach
  - Sensitivity analysis and optimisation

Multiscale method

Bridging models at different length scales

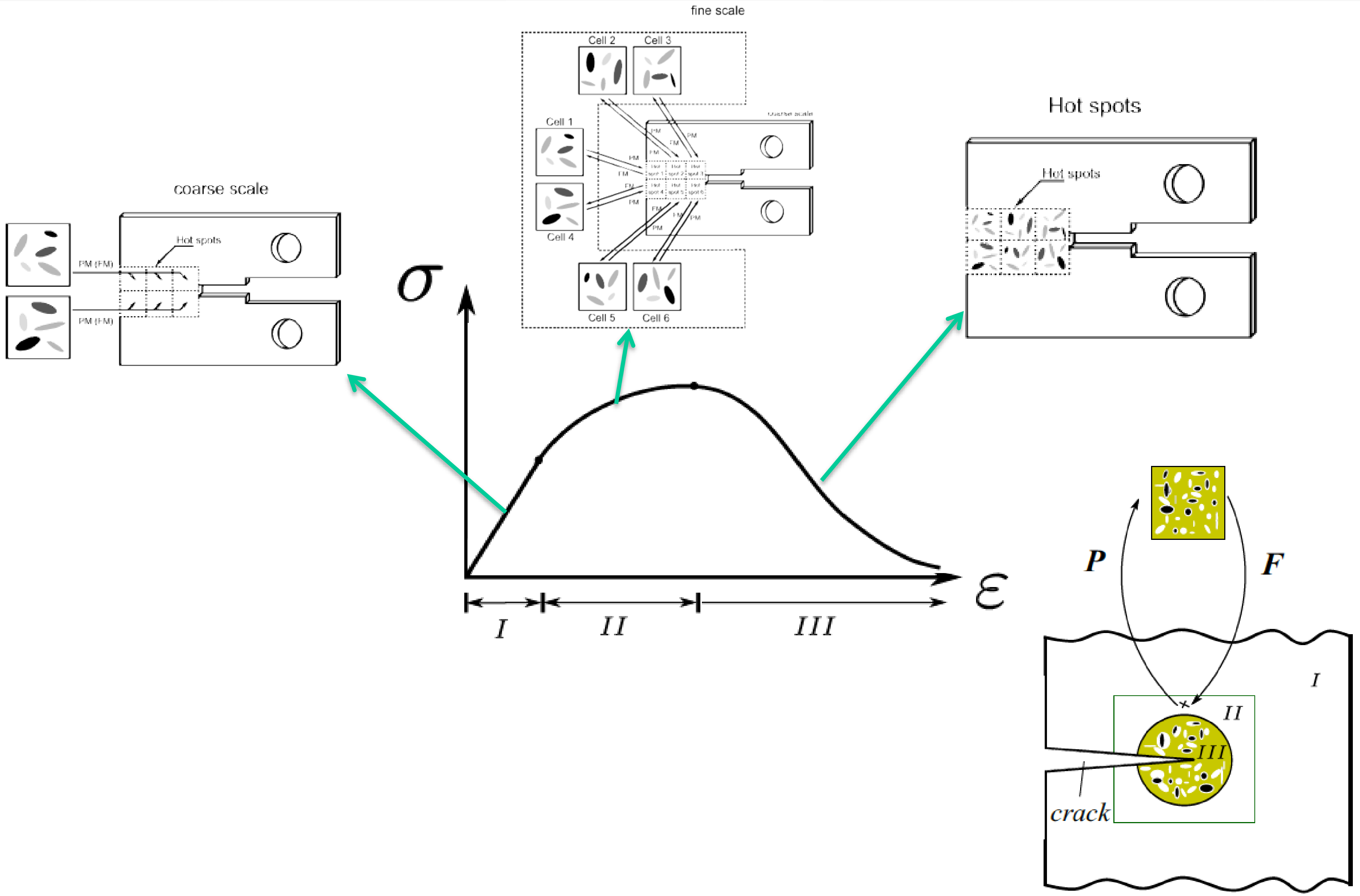

Multiscale method

Bridging models at different length scales

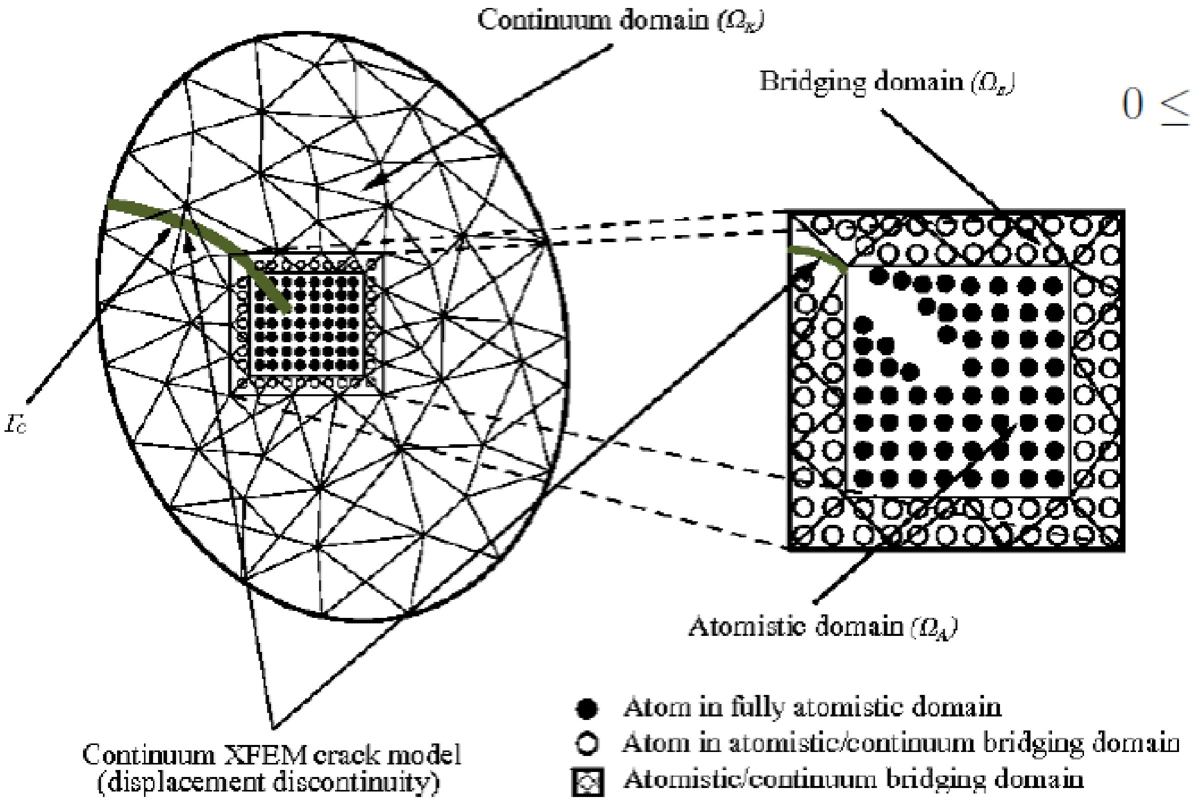

$$w^A(\mathbf{x}) + w^K(\mathbf{x}) = 1 \;\; \forall \; \mathbf{x} \in \Omega$$

$$0 \le w^i(\mathbf{x}) \le 1 \;\; , \;\; i = A, K \;\; , \;\; \forall \; \mathbf{x} \in \Omega$$

$$w^A(\mathbf{x}) = 1 \;\; \forall \; \mathbf{x} \in \Omega_A \setminus \Omega_B$$

$$w^K(\mathbf{x}) = 1 \;\; \forall \; \mathbf{x} \in \Omega_K \setminus \Omega_B$$

$$W^K(\mathbf{u}) = W^K_{int}(\mathbf{u}) + W^K_{ext}(\mathbf{u}) + W^K_{kin}(\mathbf{u})$$

$$W^K_{int}(\mathbf{u}) \;\; = \;\; \int_{\Omega^K} w^K(\mathbf{x}) \frac{1}{2} \boldsymbol{\sigma} : \boldsymbol{\epsilon} \; d\Omega$$

$$W(\mathbf{u}, \mathbf{d}^A, \boldsymbol{\lambda}) = W^K(\mathbf{u}) + W^A(\mathbf{d}^A) + W^B(\mathbf{u}, \mathbf{d}^A, \boldsymbol{\lambda})$$

$$W^B(\mathbf{u}, \mathbf{d}^A, \boldsymbol{\lambda}) = \int_{\Omega_B} \boldsymbol{\lambda} \cdot \delta\mathbf{u} \; d\Omega = \sum_{I \in \mathcal{W}^B} \int_{\Omega_B} \boldsymbol{\lambda}(\mathbf{x}) \cdot \left(\mathbf{u}(\mathbf{x}) - \mathbf{u}^A_I\right) \; \delta\left(\mathbf{x} - \mathbf{x}^A_I\right)$$

Multiscale method

Coarse graining of fractures

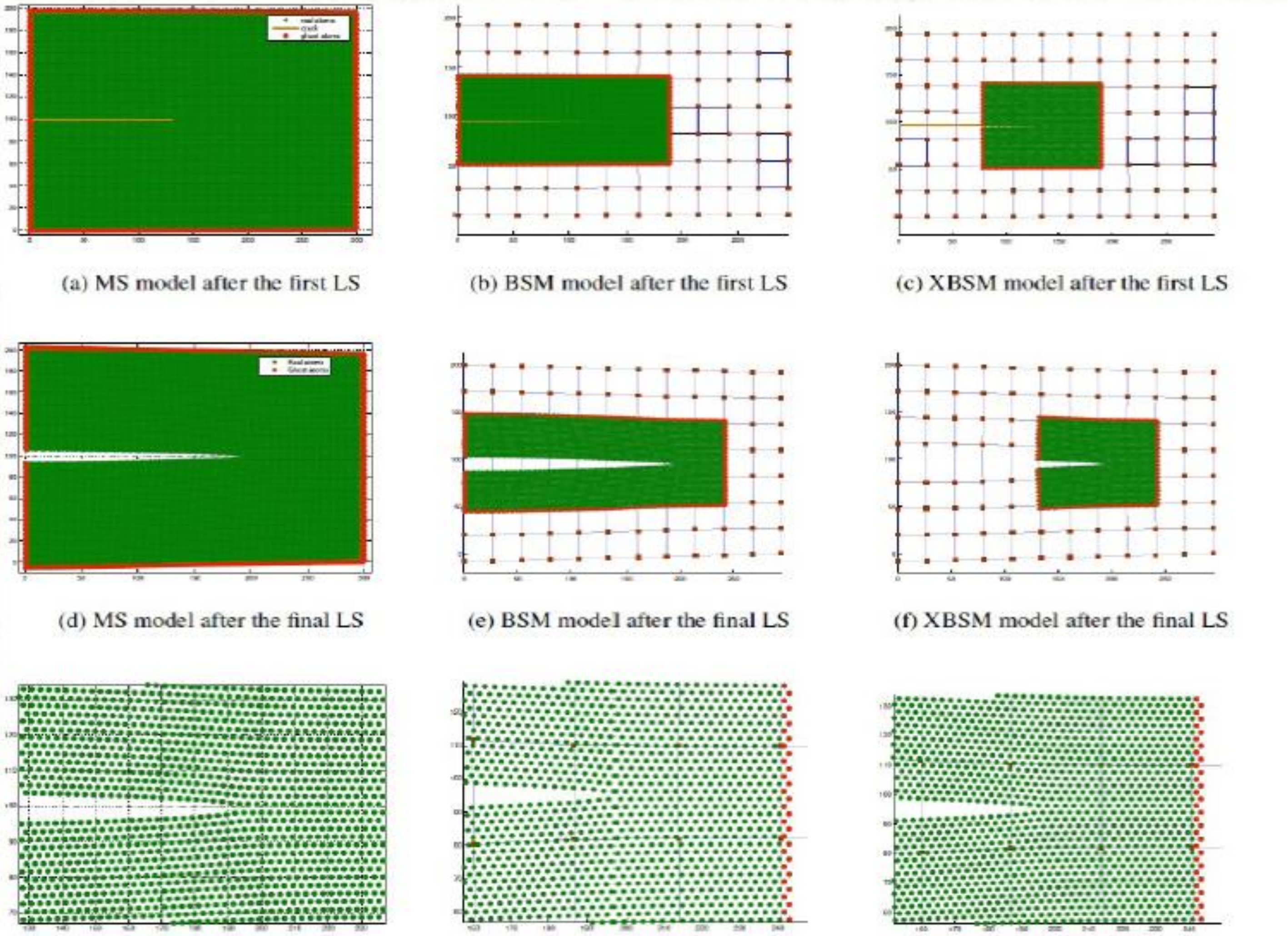

(a) MS model after the first LS
(b) BSM model after the first LS
(c) XBSM model after the first LS
(d) MS model after the final LS
(e) BSM model after the final LS
(f) XBSM model after the final LS
(g) zoom of MS model after the final LS
(h) zoom of BSM model after the final LS
(i) zoom of XBSM model after the final LS

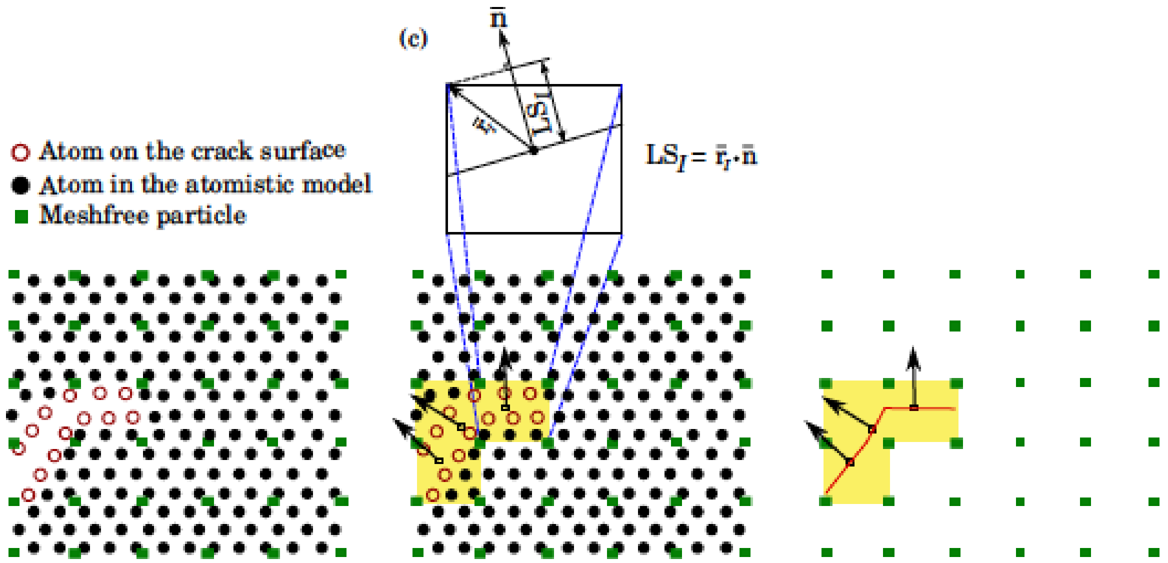

- Estimate the atoms on the crack surface (CSP).
- Calculate the normal of atoms on the crack surface.
- Identify the regions with atoms on the crack surface
- Estimate the effective normal

Budarapu P., Gracie R. Shih-Wei Y., Zhuang X., Rabczuk T.: Efficient Coarse Graining in Multiscale Modeling of Fracture, Theoretical and Applied Fracture Mechanics, 2014, 69, 126 - 143

Multiscale method

Coarse graining of fractures

$$\mathrm{CSP}_\alpha = \sum_{\beta=1}^{n^{\mathrm{nb}}/2} \left|\mathbf{r}_{\alpha\beta} + \mathbf{r}_{\alpha(\beta+n^{\mathrm{nb}}/2)}\right|^2$$

Defect	$\mathrm{csp}_\alpha / a_0^2$	Range $\Delta\mathrm{csp}_\alpha / a_0^2$
Perfect lattice	0.0000	$\mathrm{csp}_\alpha < 0.1$
Partial dislocation	0.1423	$0.01 \leq \mathrm{csp}_\alpha < 2$
Stacking fault	0.4966	$0.2 \leq \mathrm{csp}_\alpha < 1$
Surface atom	1.6881	$\mathrm{csp}_\alpha > 1$

$$\mathbf{r}_\alpha^{\mathrm{cog}} = \frac{\sum_{\beta=1}^{n^{\mathrm{nb}}} \mathbf{r}_\beta}{n^{\mathrm{nb}}}$$

$$\mathbf{n}_\alpha^{\mathrm{cog}} = \mathbf{r}_\alpha - \mathbf{r}_\alpha^{\mathrm{cog}}$$

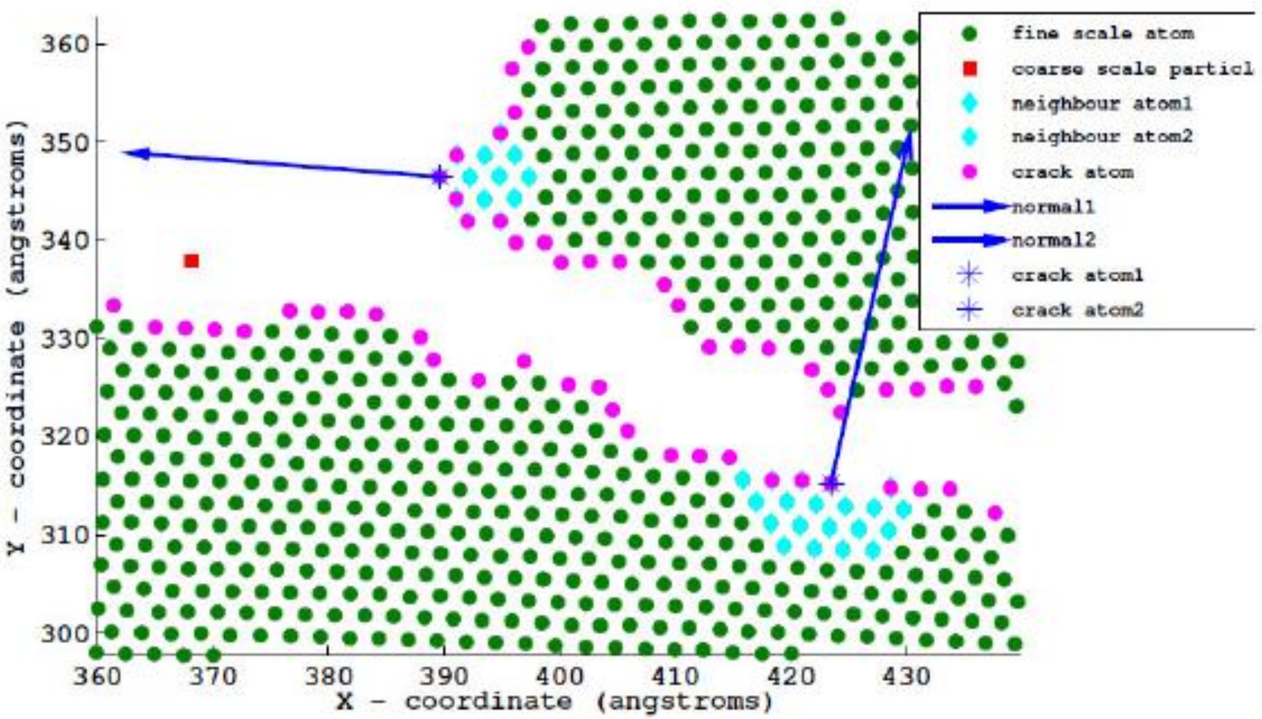

Multiscale method
Coarse graining of fractures

- Estimate the effective normal

$$\mathbf{r}_{\mathrm{cr}}^{\mathrm{cog}} = \frac{\sum_{\alpha=1}^{n^{\mathrm{cacr}}} \mathbf{r}_{\alpha}^{\mathrm{cog}}}{n^{\mathrm{cacr}}}, \qquad \mathbf{n}_{\mathrm{cr}}^{\mathrm{cog}} = \frac{\sum_{\alpha=1}^{n^{\mathrm{cacr}}} \mathbf{n}_{\alpha}^{\mathrm{cog}}}{n^{\mathrm{cacr}}}$$

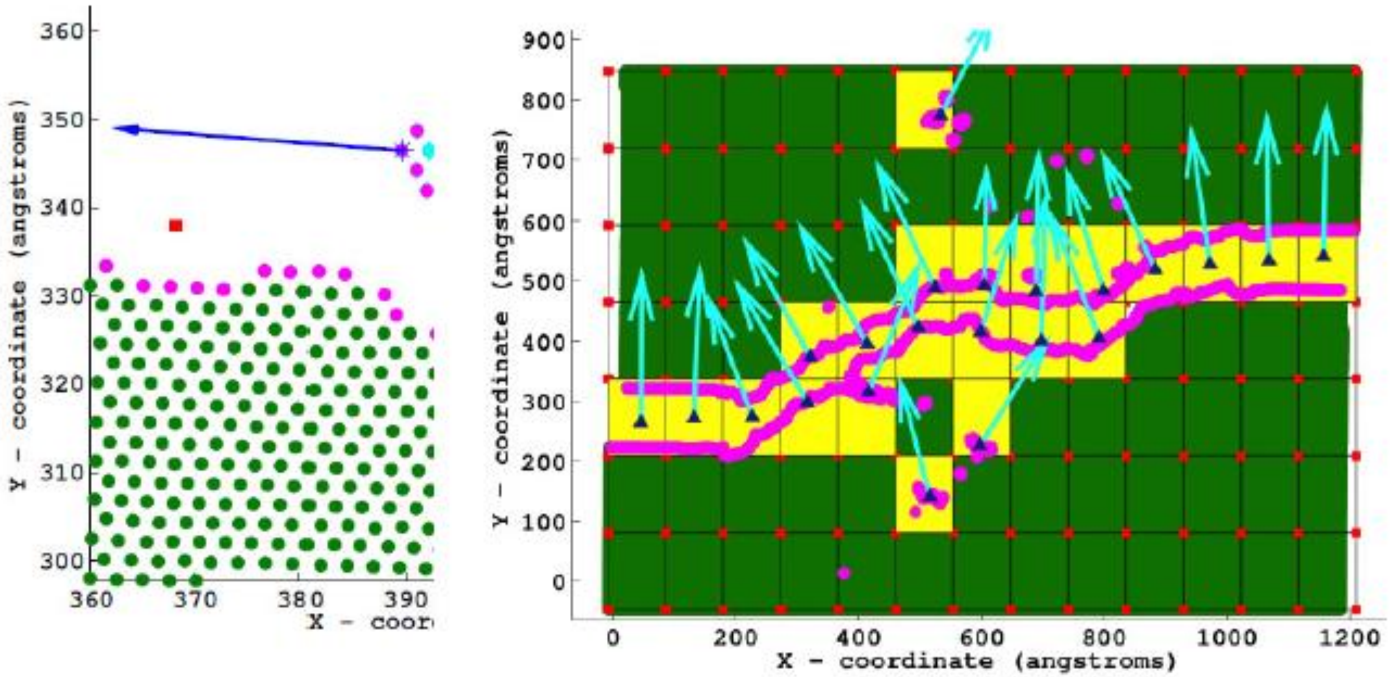

- Generate smooth crack surface

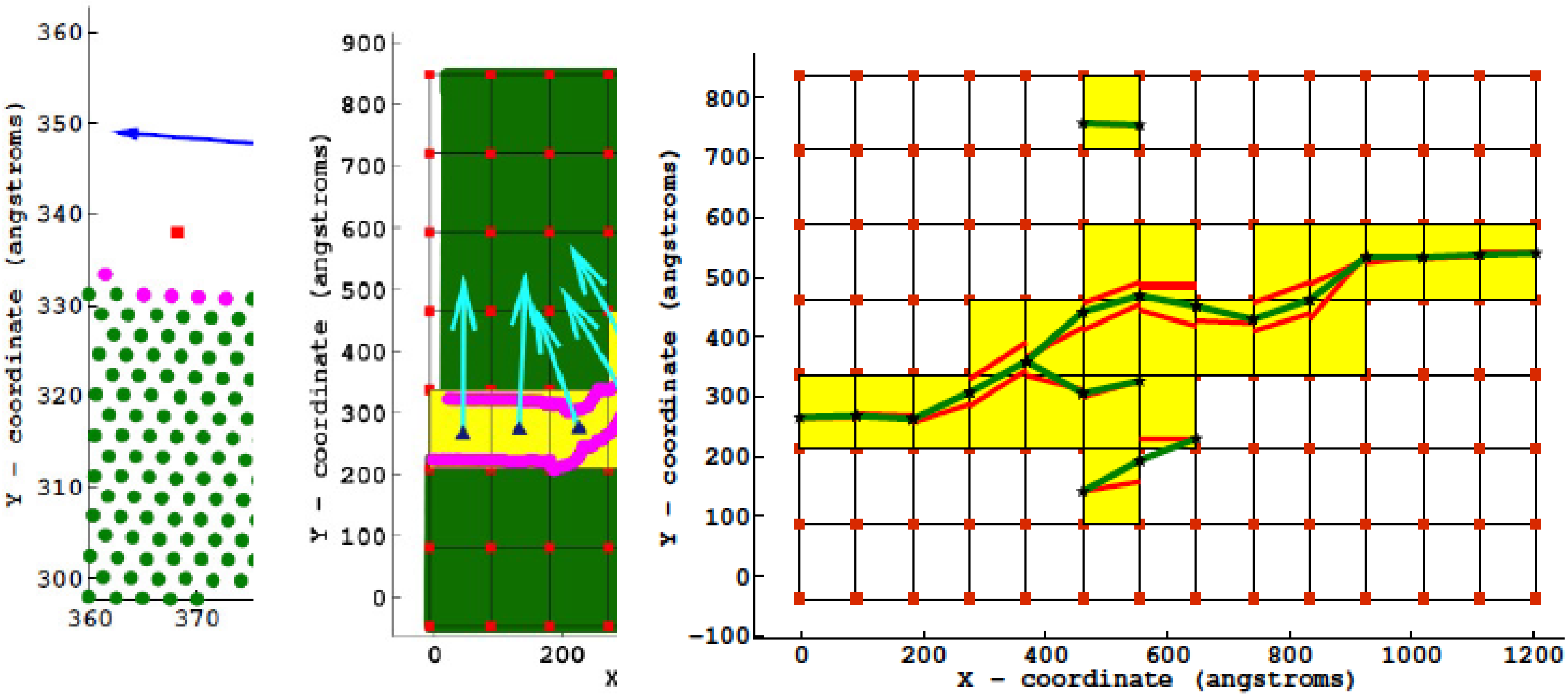

- Generate smooth crack surface

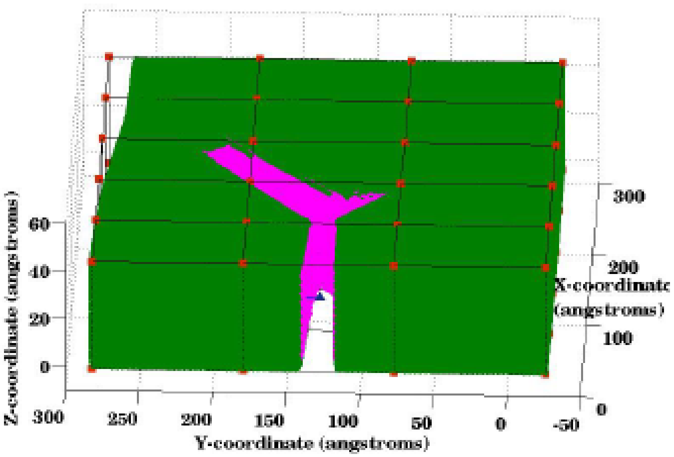

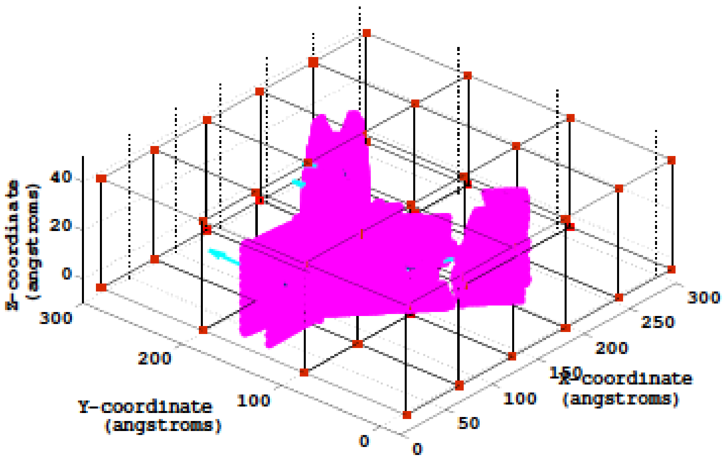

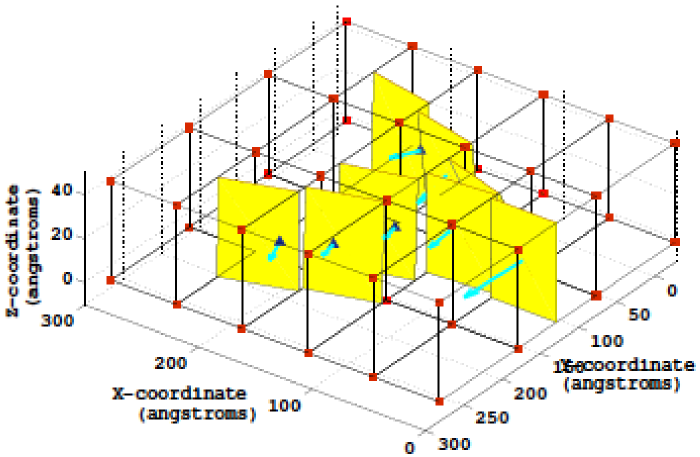

Multiscale method
Coarse graining of fractures

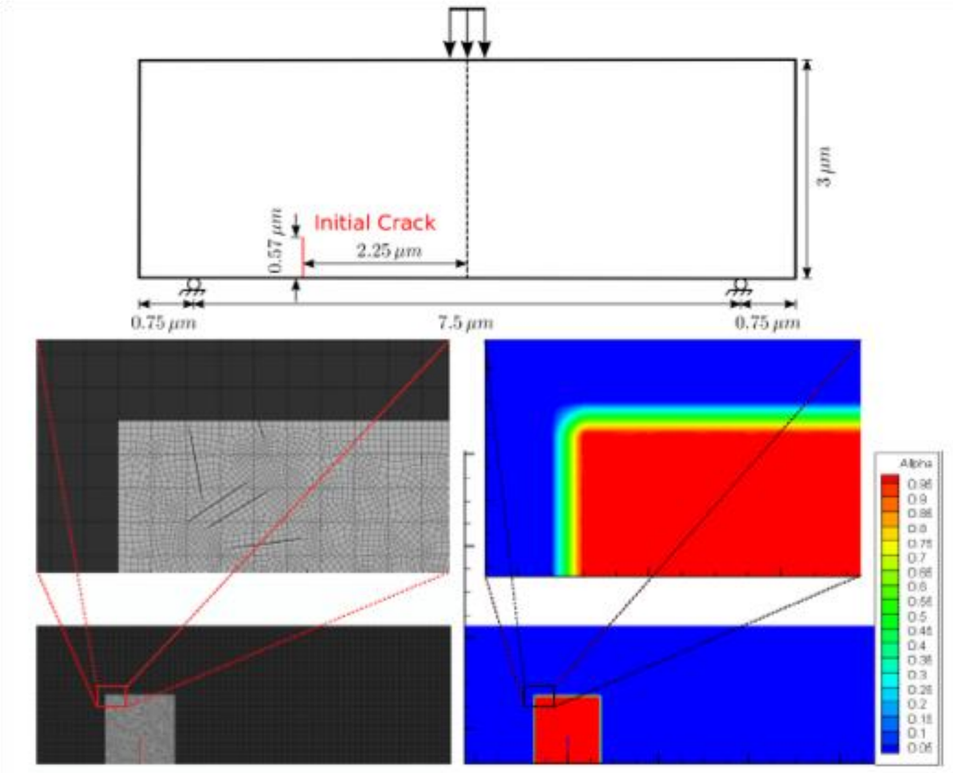

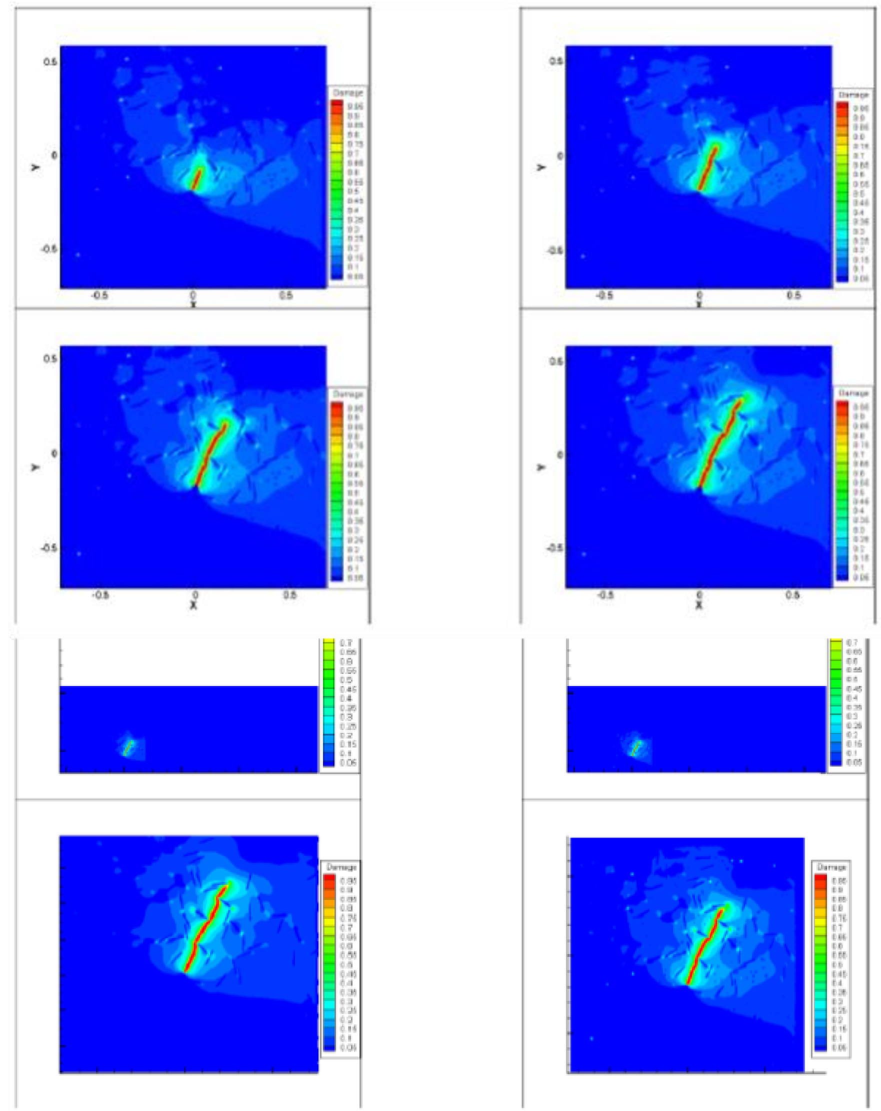

Overview

- Framework
- Computational models of polymer-matrix composites
  - Models at different length scales
  - Multiscale approach
- Uncertainty quantification and optimization
  - Sensitivity analysis
  - Probabilistic optimization

Sensitivity analysis

Nano-scale: material properties and the structure of the SWNT

Micro-scale: the SWNT embedded in the polymer matrix in the presence of the interphase is modeled and replaced by an EF

Meso-scale: the SWNT waviness, the agglomeration and the SWNT orientation

Macro-scale: the volume fraction

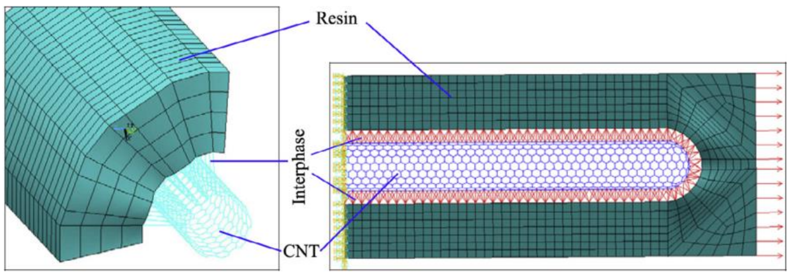

(a) Cut section of RVE (b) Side view of RVE with short CNT

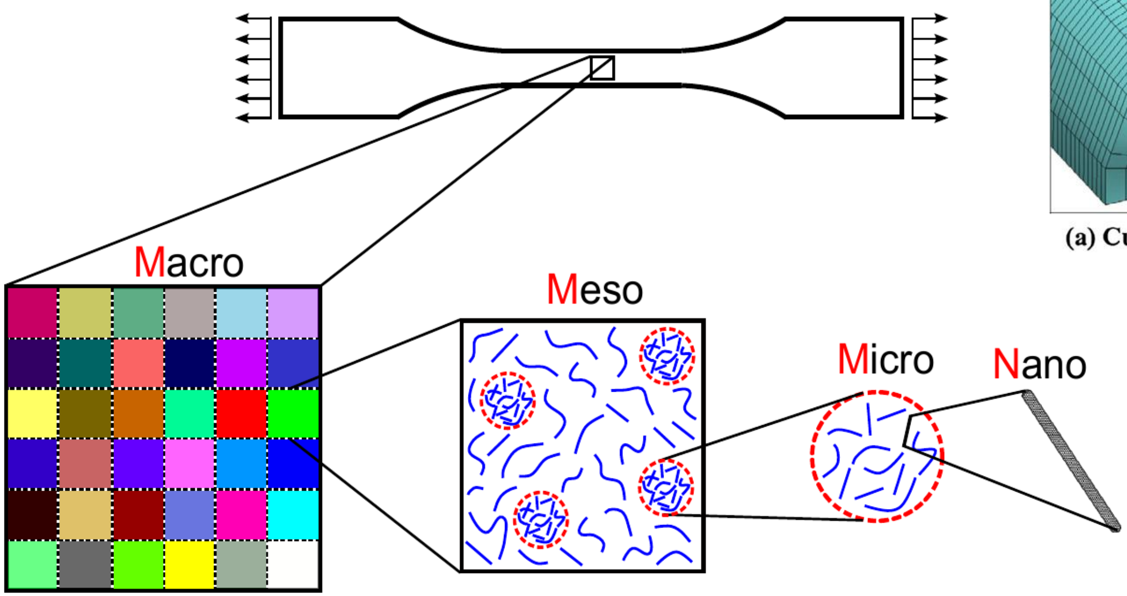

$$\xi = \frac{V^{RVE}_{inclusion}}{V^{RVE}}, \qquad \zeta = \frac{V^{r}_{inclusion}}{V^{r}},$$

$$V^r = V^r_{inclusion} + V^r_m$$

Vu-Bac N., Rafiee R., Zhuang X., Lahmer T., Rabczuk T.: Uncertainty quantification for multiscale modeling of polymer nanocomposites with correlated parameters, *Composites Part B: Engineering*, 2014, 68, 446 - 464

Sensitivity analysis

1. Sampling

MC sampling

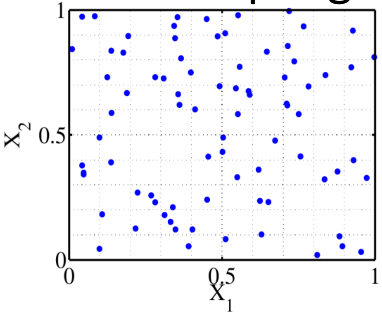

LHS sampling

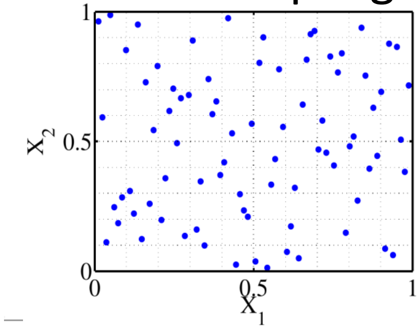

Level	Inputs	mean	standard deviation	Type of distribution
Nano/Micro	L_{SWNT} (X_1)	488.34	249.18	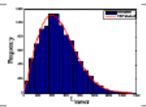
Meso	E_{LEF} (X_2)	169.18	55.85	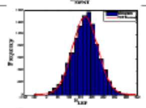
	E_{TEF} (X_3)	169.18	55.85	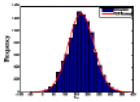
	ξ (X_4)	0.4	0.15	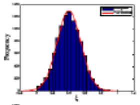
	ζ (X_5)	0.58	0.18	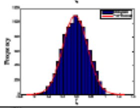
Macro	V_f (X_6)	5 %	2%	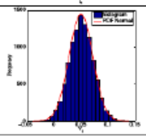

2. Surrogate Model

Quadratic regression model

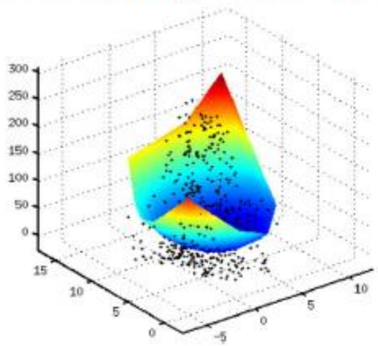

3. Sensitivity Analysis

FAST & IFAST

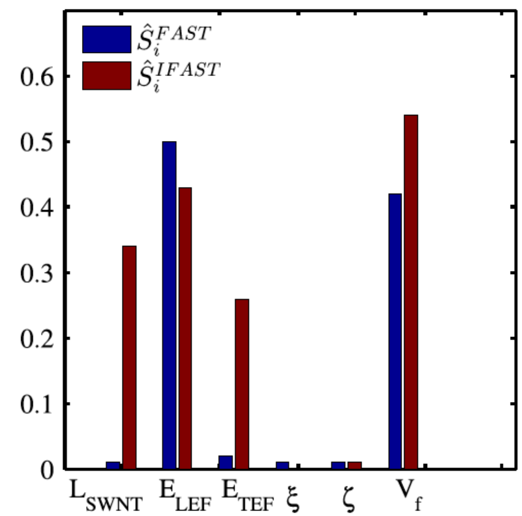

Vu-Bac N., Rafiee R., Zhuang X., Lahmer T., Rabczuk T.: Uncertainty quantification for multiscale modeling of polymer nanocomposites with correlated parameters, *Composites Part B: Engineering*, **2014**, 68, 446 - 464

Probabilistic optimization

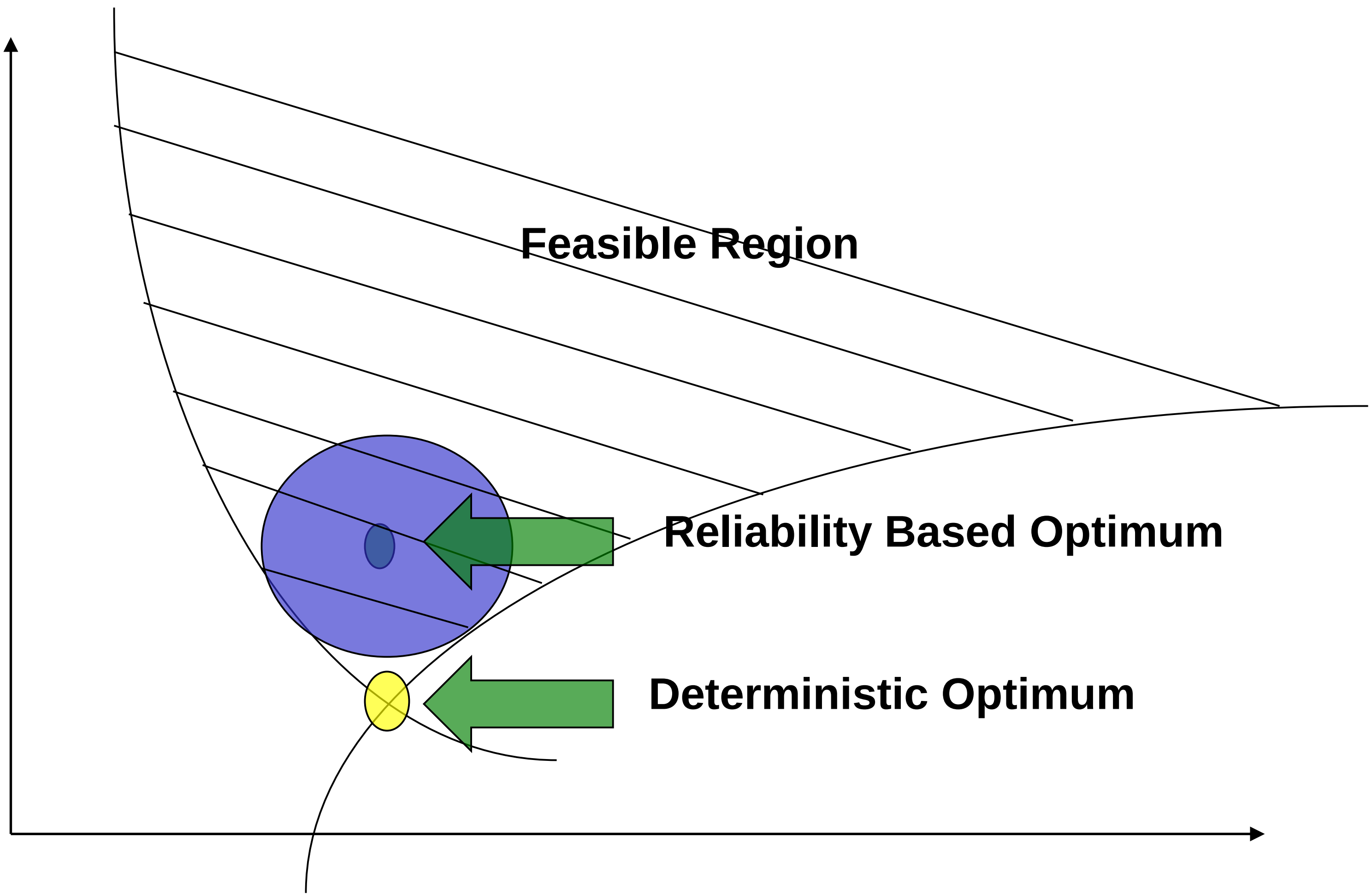

Probabilistic optimization

Thick cylinder subjected to line load

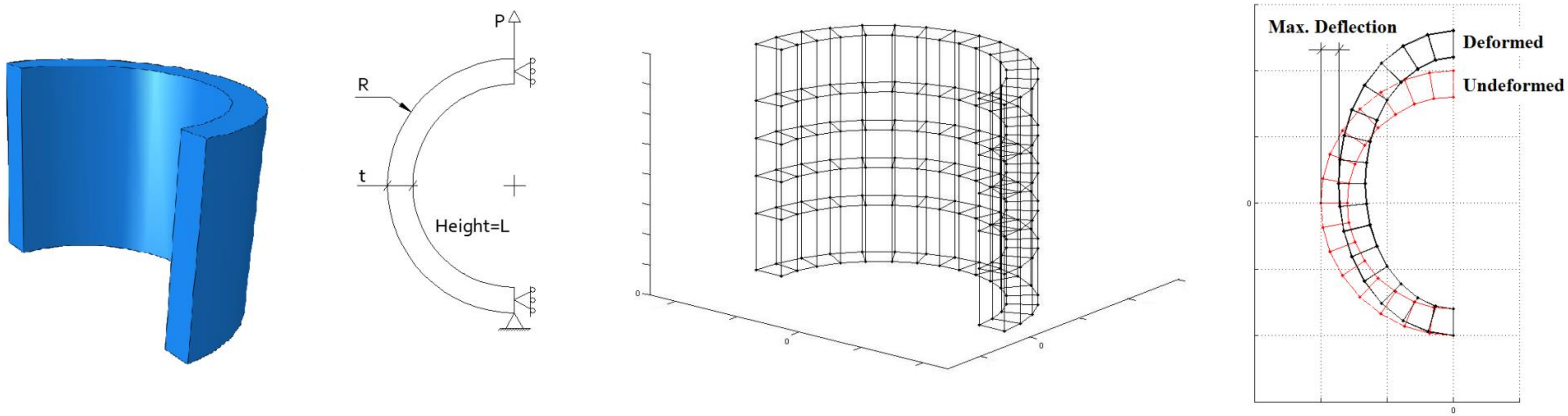

a) b) c) d)

Parameter	R_c	L_c	E_m	ν_m	P	LSF	β	$Obj. Func.$
Value	1	1.5	10	0.3	$\mu = 1000$ $\sigma = 200$	Max. trans. deflect. $7\ e^{-3}$	3	% CNT + t_c
Type	D	D	D	D	N	D	D	D

$Length: m,\ \ E: GPa\ ,\ \ P: Applied\ load\ (KN/m),\ \ \nu: Poisson\ ratio,\ \ m: matrix,\ \ c: cylinder$

$D: deterministic, N: normal\ distribution, \mu: mean\ value, \sigma: standard\ deviation\ \ \beta: Reliability\ Index$

1% < volfrac% < 10% & 0.1 < t_c < 0.4

Minimization of the CNT content and the cylinder thickness simultaneously

a)

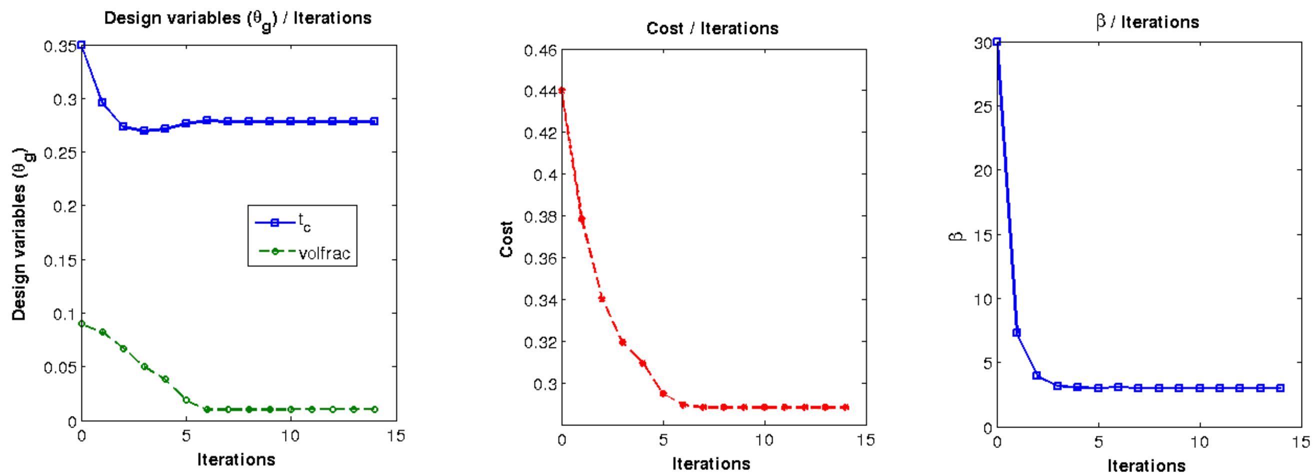

b)

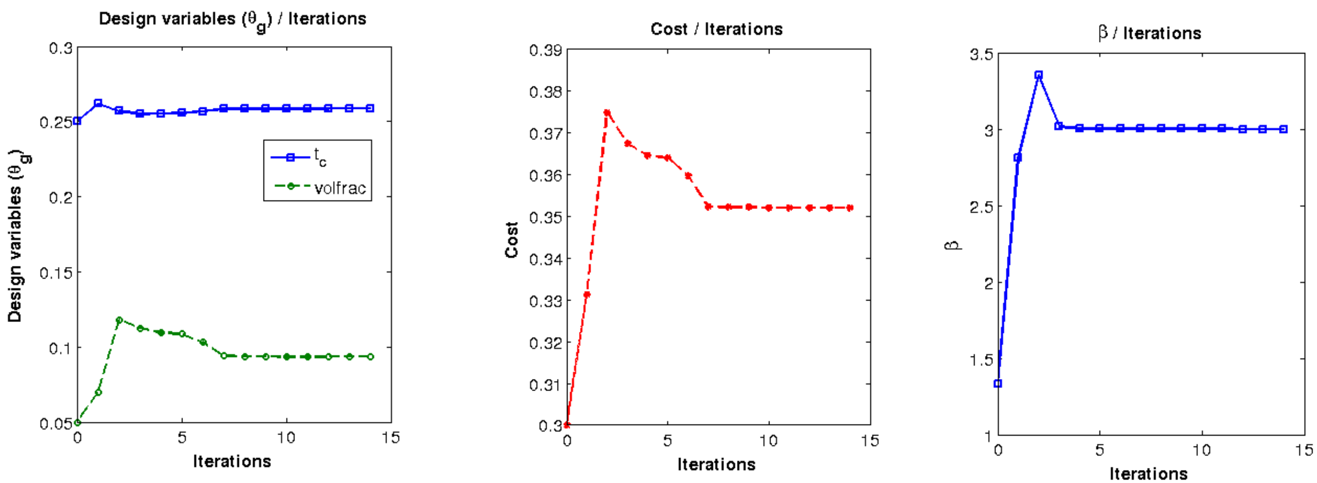

Thank you for your attention!